

# A Comprehensive Assessment of CFS Seasonal Forecasts over the Tropics\*

K. P. SOORAJ AND H. ANNAMALAI

*International Pacific Research Center, School of Ocean and Earth Science and Technology,  
University of Hawaii at Manoa, Honolulu, Hawaii*

ARUN KUMAR

*NCEP/Climate Prediction Center, Washington, D.C.*

HUI WANG

*NCEP/Climate Prediction Center Washington, D.C., and Wyle Information Systems, McLean, Virginia*

(Manuscript received 4 February 2011, in final form 22 August 2011)

## ABSTRACT

The 15-member ensemble hindcasts performed with the National Centers for Environmental Prediction Climate Forecast System (CFS) for the period 1981–2005, as well as real-time forecasts for the period 2006–09, are assessed for seasonal prediction skills over the tropics, from deterministic (anomaly correlation), categorical (Heidke skill score), and probabilistic (rank probability skill score) perspectives. Further, persistence, signal-to-noise ratio, and root-mean-square error analyses are also performed. The CFS demonstrates high skill in forecasting El Niño–Southern Oscillation (ENSO) related sea surface temperature (SST) anomalies during developing and mature phases, including that of different types of El Niño. During ENSO, the space–time evolution of anomalous SST, 850-hPa wind, and rainfall along the equatorial Pacific, as well as the mechanisms involved in the teleconnection to the tropical Indian Ocean, are also well represented. During ENSO phase transition and in the summer, the skill of forecasting Pacific SST anomalies is modest. An examination of CFS ability in forecasting seasonal rainfall anomalies over the U.S. Affiliated Pacific Islands (USAPI) indicates that forecasting the persistence of dryness from El Niño winter into the following spring/summer is skillful at leads > 3 months. During strong El Niño years the persistence is predicted by all members with a 6-month lead time. Also, the model is skillful in predicting regional rainfall responses during different types of El Niño. Since both deterministic and probabilistic skill scores converge, the suggestion is that the forecast is useful. The model's skill in the real-time forecasts for the period 2006–09 is also discussed. The results suggest the feasibility that a dynamical-system-based seasonal prediction of precipitation over the USAPI can be considered.

## 1. Introduction

### *a. Background*

With a substantial portion of the world's population influenced by climate variability, such as drought, flood,

heat, and cold waves, any capability to anticipate these fluctuations one or more seasons ahead would have measurable benefits for decision making in many sectors of society (Mason et al. 1999; Gong et al. 2003; Palmer et al. 2004; Barnston et al. 2005). From the early 1980s to late 1990s, improvements in coupled climate models have led to the ability to predict tropical climate variations with some success (Kang and Shukla 2006; Kirtman and Pirani 2009). Here, we examine the seasonal forecast performance of the National Centers for Environmental Prediction's (NCEP) Coupled Forecast System (CFS) over the tropics and also over the U.S. Affiliated Pacific Islands (USAPI).

The hypothesis that boundary conditions such as sea surface temperature (SST), snow cover, and soil wetness

---

\* International Pacific Research Center Publication Number 815 and School of Ocean and Earth Science and Technology Publication Number 8531.

---

*Corresponding author address:* Dr. H. Annamalai, IPRC, SOEST, University of Hawaii at Manoa, 1680 East–West Rd., Honolulu, HI 96822.  
E-mail: hanna@hawaii.edu

have significant influence on seasonal mean tropical circulation and rainfall (Charney and Shukla 1981) has been supported by various atmospheric general circulation model (AGCM) sensitivity studies (e.g., Shukla and Wallace 1983; Livezey et al. 1996; Kumar and Hoerling 1998). In particular, Shukla (1998) showed that the tropical flow patterns and rainfall over the Pacific are determined by the underlying SST, as was also suggested by Soman and Slingo (1997). In summary, seasonal prediction over the tropics, and to a certain degree over the extratropics, are essentially linked to the accurate prediction of tropical SST (Goddard et al. 2001). Due to their impacts on global climate anomalies (Ropelewski and Halpert 1987), predicting SST variations during the life cycle of El Niño–Southern Oscillation (ENSO) has been the focus of coupled model development. Many recent studies have assessed ENSO simulations in coupled general circulation models (CGCMs; Jin et al. 2008; AchutaRao and Sperber 2006; Guilyardi et al. 2004, and the references therein).

While efforts are under way to reduce model systematic errors, many CGCMs have shown skill in capturing ENSO characteristics, paving ways for routine operational seasonal forecasts (Anderson et al. 2003; Van Oldenborgh et al. 2005a; Saha et al. 2006). Recent studies have evaluated the skill of models to forecast ENSO by analyzing hindcasts produced by CGCMs. Jin et al. (2008) noted that the skill of a single model or ensemble of models depends on the season, phase, and amplitude of ENSO. Luo et al. (2008, 2010) noted high skill in forecasting both ENSO and the Indian Ocean dipole zonal mode (IODZM). Despite success, the predictive skills of models are degraded during the ENSO onset and decay periods (Barnston et al. 1999; Clarke and Van Gorder 2003). The latest version of the European Centre for Medium-Range Weather Forecasts's (ECMWF) seasonal forecast system (S3) demonstrated improvements in the overall skill of ENSO forecasts, which can be partly attributable to improvements in observing systems in recent decades (Stockdale et al. 2011).

With regard to the CFS, Saha et al. (2006) presented the overall model characteristics and pointed out that the forecast skill over the Niño-3.4 region ( $5^{\circ}\text{S}$ – $5^{\circ}\text{N}$ ,  $170^{\circ}$ – $120^{\circ}\text{W}$ ) is comparable to statistical methods used at NCEP up to a 6-month lead. Jin and Kinter (2009) performed a comprehensive study exploring the error growth that masks the predictability of ENSO. The authors attributed the degradation of the skill (after the impacts of initial uncertainties fade out) to the systematic errors in the control simulations. The skill in hindcasting the peak phase of IODZM in boreal fall rests on the uncertainties in forecasting the south Asian monsoon circulation (Wajsovicz 2005).

Theoretical and modeling studies have demonstrated that ENSO owes its existence to unstable ocean–atmosphere interactions in the tropical Pacific (Battisti 1988; Neelin et al. 1998), and its statistical properties such as amplitude and phase transition may be influenced by high-frequency stochastic forcing (Kessler et al. 1995), and precipitation variations over the tropical Indian Ocean–Indonesian Seas region (Anderson and McCreary 1985; Wu and Kirtman 2004; Annamalai et al. 2005b, 2010; Kug and Kang 2006). While it is recognized that ENSO influences global climate anomalies, sensitivity experiments with AGCMs suggest that SST variations over the southwest Indian Ocean (SWIO) also modulate the amplitude of ENSO-induced circulation and precipitation anomalies over the tropical west Pacific (Watanabe and Jin 2003; Annamalai et al. 2005a), and over the Pacific–North American (PNA) region (Annamalai et al. 2007). However, these regional SST anomalies are influenced by ENSO itself through the atmospheric bridge (Klein et al. 1999) and through local ocean Rossby waves, which in turn are forced by ENSO-related wind anomalies over the equatorial Indian Ocean (Xie et al. 2002; Huang and Kinter 2002). During strong IODZM events, due to ocean Rossby waves, thermocline and SST variations over SWIO are also modified (Rao et al. 2002). In summary, the expectation is that the combined effects of the tropical Pacific and Indian Oceans can further strengthen global climate anomalies.

Recent research interests have also focused on two types of El Niño events, namely, western Pacific and cold-tongue events. While the mechanisms responsible differ (Larkin and Harrison 2005a,b; Wang and Hendon 2007; Kug et al. 2009; Kao and Yu 2009), it is desirable to check CFS's skill in forecasting these two categories, or different types, of El Niño.

For the target regions over the USAPI (Fig. 1), the current operational seasonal precipitation prediction system is based on empirical methods in which SSTs provide the predictive information, and higher prediction skill is noticed during ENSO winters (He and Barnston 1996). During non-ENSO and weak-to-moderate ENSO events too, the USAPI experience significant seasonal rainfall anomalies (section 3d). In these circumstances, the precipitation forecast skill of the empirical model is low, and the reasons may be manifold including (a) the nonlinear relationship between ENSO SST and precipitation is not incorporated, (b) details in the space–time evolution of SST during different types of ENSO are not properly accounted for, and (c) SST anomalies other than ENSO may be responsible for rainfall variations. A prediction system based on a fully coupled dynamical model may overcome some of the above limitations.

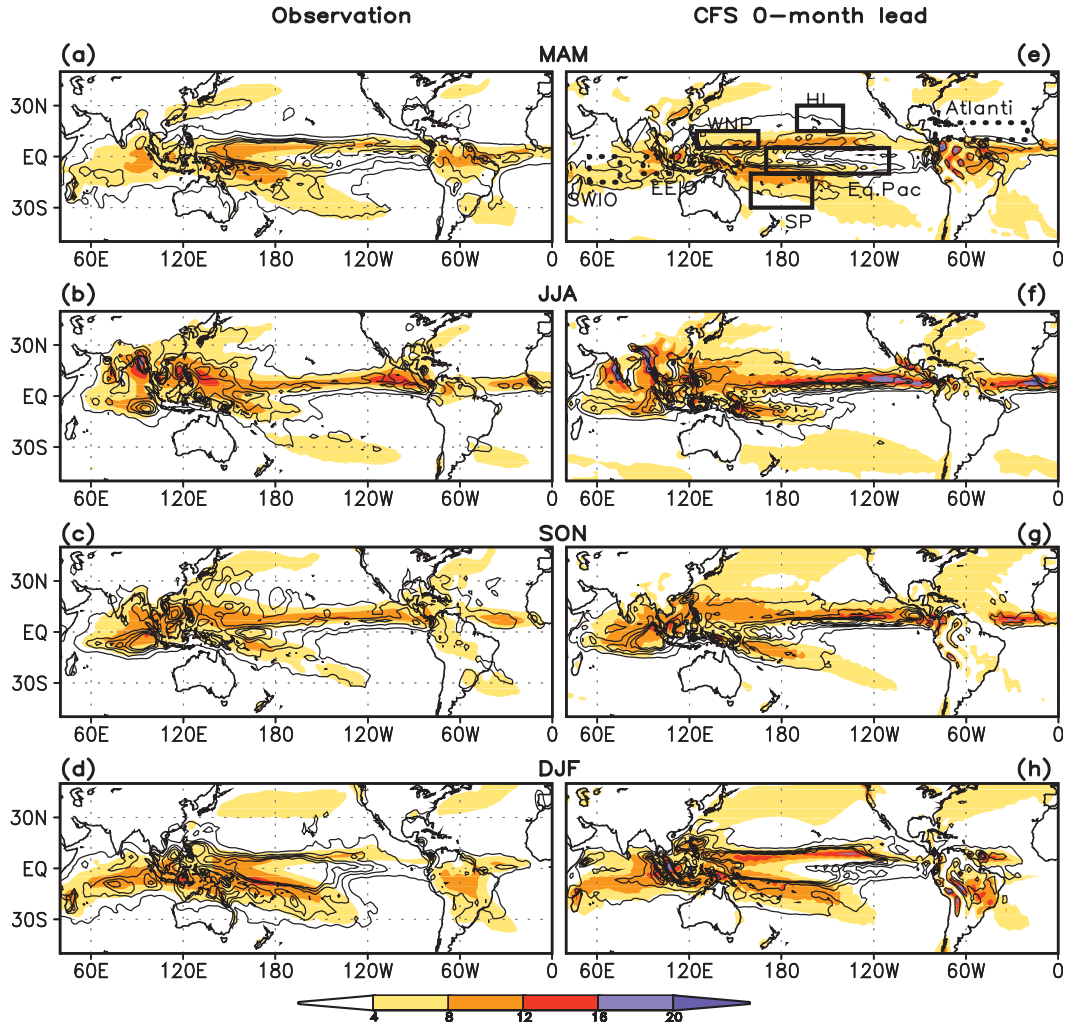


FIG. 1. Climatological precipitation ( $\text{mm day}^{-1}$ , shaded) and variance ( $\text{mm}^2 \text{day}^{-1}$ , contours) for four standard seasons from (a)–(d) observations and (e)–(h) the 0-month CFS forecast. The boxed areas in (e) represent the regions where CFS’s ability to forecast seasonal SST or precipitation anomalies is assessed. The area-averaging regions used are SWIO ( $15^{\circ}\text{S}$ – $0^{\circ}$ ,  $55^{\circ}$ – $75^{\circ}\text{E}$ ), EEIO ( $10^{\circ}\text{S}$ – $0^{\circ}$ ,  $90^{\circ}$ – $110^{\circ}\text{E}$ ), the northern Atlantic ( $10^{\circ}$ – $20^{\circ}\text{N}$ ,  $20^{\circ}$ – $80^{\circ}\text{W}$ ), the WNP ( $5^{\circ}$ – $15^{\circ}\text{N}$ ,  $125^{\circ}$ – $155^{\circ}\text{E}$ ); SP ( $10^{\circ}$ – $30^{\circ}\text{S}$ ,  $160^{\circ}$ – $200^{\circ}\text{E}$ ), HI ( $15^{\circ}$ – $30^{\circ}\text{N}$ ,  $140^{\circ}$ – $170^{\circ}\text{W}$ ), and EPAC ( $10^{\circ}\text{S}$ – $5^{\circ}\text{N}$ ,  $170^{\circ}$ – $110^{\circ}\text{W}$ ). Contours are drawn starting from  $1 \text{ mm}^2 \text{day}^{-1}$  with an interval of 2 units.

*b. Present study*

Here, we evaluate seasonal skills using 15-member ensemble retrospective forecasts (or hindcasts) performed with the CFS for the period 1982–2005. Hindcasts can identify systematic errors of the forecast system and provide estimates of skill information to the user. The CFS skill is also evaluated for the real-time forecast for the period 2006–09 (Wang et al. 2010).

Figure 1 shows climatological precipitation (shaded) and variance (contours) for standard seasons from observations (Fig. 1, left) and at 0-month lead hindcast from CFS (Fig. 1, right). Compared to observations, CFS captures the seasonal dependency in the position and

intensity of the rainfall maximum and also the regional variance maxima over the tropics with some systematic errors. Motivated by this, and apart from examining SST skill over the equatorial Pacific, we also evaluate CFS’ ability in forecasting (i) tropical and regional precipitation anomalies, (ii) different types of El Niño and their associated regional responses, and (iii) teleconnection between the tropical Pacific and Indian Oceans (TIO). In terms of regional indices, skill is examined for precipitation (area outlined by solid lines in Fig. 1), and SST influenced by thermocline variations over the TIO (area outlined by dotted lines in Fig. 1). The model’s skill in forecasting northern tropical Atlantic SST anomalies is also examined. To infer the uncertainty measures

associated with forecasts, the skills are assessed using deterministic, categorical, and probabilistic methods.

In the remainder of this paper, section 2 provides a brief description of CFS, the hindcasts analyzed, and the verification tools. In section 3, deterministic skill and the associated errors over the target regions are presented. Section 4 deals with assessments of different aspects of the forecasts. Section 5 is devoted to the analysis of real-time forecasts, and section 6 provides the implications of the present results on seasonal predictions of regional precipitation. Section 7 provides the summary.

## 2. Model hindcasts, forecasts, and verification methods

### a. CFS hindcasts and real-time forecasts

CFS is a fully coupled dynamical prediction system and has been an important component of the monthly to seasonal prediction system of the NCEP's Climate Prediction Center (CPC) since it became operational in 2004 (Saha et al. 2006). The atmospheric and oceanic components are coupled without flux adjustment and the two components exchange time-averaged quantities once a day. Full atmosphere–ocean interaction is confined to 65°S–50°N. The readers are referred to Saha et al. (2006) for more details on model configurations.

Here, we analyze the output from the CFS retrospective predictions (or alternatively referred to as hindcasts) that cover all 12 calendar months from 1981 to 2005. These hindcast runs, each of which is a 9-month integration, are ensembles of 15 members starting from perturbed real-time oceanic and atmospheric initial conditions (ICs) from the NCEP Global Ocean Data Assimilation (D. Behringer 2005, personal communication) and the NCEP–Department of Energy Atmospheric Model Intercomparison Project II Reanalysis (Kanamitsu et al. 2002), respectively. For the hindcasts starting from a specific month (e.g., May ICs), the ICs for the 15 members in the ensemble include 9–13 May, 19–23 May, and 30 May–3 June. Note that, for a 9-month integration, prediction at 6-month lead (L6) is the longest lead available for seasonal means while 8-month lead (L8) is the longest for monthly means. Variables examined include SST, precipitation, and wind at 850 hPa. To infer the ocean Rossby waves in the TIO, we also analyzed sea surface height (SSH). Hindcast anomalies are computed by removing the model climatology for each grid point, each initial month, and each lead time from the original ensemble hindcasts. The hindcast data used in our analysis are not the type available to the external users via public download. Essentially after the original set of hindcast was completed, and the data were made publically available, hindcasts from 1981 to 1990

were repeated to correct an error in the ocean analysis that provided the ocean initial conditions. The error resulted in too warm SSTs during 1981–90, and requires detrending of the original hindcast data. Regarding verification of the real-time forecasts for the period 2006–09, we examined a 15-member ensemble corresponding to the same ICs as in the hindcasts. The real-time forecast anomalies were calculated based on 1981–2004 climatology.

For the period 1981–2009, observed datasets used for verification include the CPC Merged Analysis of Precipitation (CMAP; Xie and Arkin 1996), winds from the NCEP–DOE reanalysis (Kanamitsu et al. 2002), and the National Oceanic and Atmospheric Administration's (NOAA) optimally interpolated SST analysis (Reynolds et al. 2002). SSH is taken from the Global Ocean Data Assimilation System. For verification, observed data are interpolated to CFS's horizontal resolution (T62).

### b. Verification methods

The entire range of available hindcasts (0–6-month lead) for all four standard seasons is verified. The multitude of verification measures includes deterministic, categorical, and probabilistic skill scores. The anomaly correlation coefficient (ACC), ensemble spread, and signal-to-noise ratio (S/N) are estimated. Additionally, the skill of the persistence forecast and root-mean-square error (RMSE) are calculated. For the target regions (Fig. 1), the distribution of ensemble members, the ensemble mean, and the observed anomaly are plotted for every year. These plots help in understanding the year-to-year variations in the spread and its association with the predicted value, and whether there is asymmetry in the model's predictive skill (for positive versus negative values).

To verify multicategory forecasts, the Heidke skill score (HSS) is employed. The probabilistic forecasts are evaluated using the rank probability skill score (RPSS). A brief description of them is provided here, while the appendix provides more details of the methods:

- 1) ACC—For the ensemble mean as the deterministic forecast from dynamical seasonal prediction methods, the anomaly correlation between observed and forecast time series as a measure of deterministic prediction skill is computed. Here, ACC is estimated between the ensemble means of the forecast and the observations, as well as between individual members and observations.
- 2) HSS—For categorical forecasts, HSS measures the forecast success rate (hits versus misses) relative to a random guess as the forecast (Wilks 1995). The measure is based on a tercile classification (above normal, normal, and below normal), and the score (expressed as a percentage) indicates the accuracy of



the forecast in predicting the correct category relative to that of a random guess as the forecast (i.e., climatological probability or equal chance for each tercile). A score of 0 means that the forecast did no better than the climatological probabilities as the forecast. A score of 100 depicts a perfect forecast and a score of  $-50$  depicts the worst possible forecast.

- 3) RPSS—This metric is intended to assess the skill of probabilistic forecasts (Goddard et al. 2003). Specifically, RPSS is a measure of the square of the difference in the cumulative forecast and the observed probability for each category, and penalizes for forecasting the wrong category. The RPSS is usually expressed as a percentage and a negative value implies that the forecast is less skillful than climatology. For typical climate forecasts with modest skill, for which forecast probabilities typically fall within 20% of their climatological values (33.3%), RPSS scores are often in the range of 5%–20%.
- 4) S/N—Signal to noise ratio is estimated as the ratio of the interannual standard deviation of a 15-member ensemble mean to the spread, where spread is defined as the interensemble standard deviation of the 15 members (Kumar and Hoerling 1995).

### 3. Deterministic skill over the tropical Pacific and Indian Oceans

A prerequisite for successful seasonal forecasts is an ability to predict accurately the state of the ocean. In this section, at all lead times, and for forecasts initialized in all months, the model's SST skill over the Niño-3.4, Niño-4, and Niño-3 regions are first evaluated (section 3a), as is the precipitation skill over the equatorial Pacific (section 3b). The teleconnection between the tropical Pacific and Indian Ocean, together with the representation of TIO local oceanic processes, are examined (section 3c). In section 3d, skill in forecasting Atlantic SST is presented. Finally, the model's skill in forecasting rainfall anomalies over the USAPI is presented (section 3e).

#### a. SST over the equatorial Pacific

Figure 2 shows the ACC (Fig. 2a) and RMSE (Fig. 2c) for Niño-3.4 SST anomalies. Results are shown for all lead times (0–8 months), and for all ICs (January–December). The corresponding measures estimated from the persistence forecast are shown in Figs. 2b,d. The inverse association between ACC and RMSE holds, and the ensemble mean offers a higher level of skill than persistence. For instance, for leads up to 6–7 months and hindcasts initialized during late spring through early fall (May–October), the ensemble mean ACC is  $> 0.8$  with

a relatively small RMSE (0.3–0.4) but for the persistence forecast the ACC drops below 0.6 with a higher RMSE ( $\sim 0.7$ –0.8). This means that the skill in forecasting the intensification and peak amplitude of ENSO is indeed high. However, for forecasts initialized during winter (November–January), the skill for the transition phase of ENSO is modest at best. Specifically, both methods share similar ACC and RMSE values in the first 3–5 months (Figs. 2a–d), but they drop off rapidly during spring with a minimum in July. This decay in skill, often referred to as the spring predictability barrier, is common to most models (Clarke and Van Gorder 1999; Wu et al. 2008; Jin and Kinter 2009; Stockdale et al. 2011). The results presented here based on ICs versus lead months are consistent with those estimated from target months versus lead months (Saha et al. 2006). The forecast performance of CFS over the Niño-3.4 region is comparable to that of the ECMWF S3 system (Stockdale et al. 2011).

ENSO prediction is further assessed in four different ways. First, the model's relative skill in hindcasting individual El Niño and La Niña events (Fig. 3a) is evaluated for the peak phase (December–February, DJF) at 0-month lead. This is necessitated because observations during the period 1982–2005 indicate unique features that models need to forecast. They include (i) two of the strongest El Niño events of the twentieth century (1982 and 1997) and (ii) persistent La Niña conditions during 1998–2000 (thick red circles in Fig. 3a). It is encouraging that all the ensemble members (green circles) capture correctly the amplitude during 1982 and 1997, and the model's ability in hindcasting these two events is remarkable even for leads up to 6 months (Fig. 4a). For the prolonged La Niña episode, however, the predicted amplitude is higher in conjunction with a larger ensemble spread. It is also encouraging that the model is able to correctly forecast near-normal conditions in many years. Van Oldenborgh et al. (2005a) noted that the hindcasts produced by the ECMWF seasonal forecast system (S1 and S2) were unable to capture the amplitude of the 1987 and 1997 warm events, but the extended cold event (1998–2000) was forecast correctly. On the other hand, at short leads the new system (S3) demonstrated high skill in forecasting the amplitudes of these warm events but the details were not correct for cold events; however, for longer leads, forecasting the peak amplitude during 1982 met with moderate success (Stockdale et al. 2011).

Second, to understand the skill dependence as a function of seasons, Table 1a summarizes the statistics for Niño-3.4 at various leads and for all the four seasons. While ACC remains high for the fall, winter, and spring seasons, the skill drops off markedly for summer at longer lead times. Even for DJF while ACC remains around 0.9

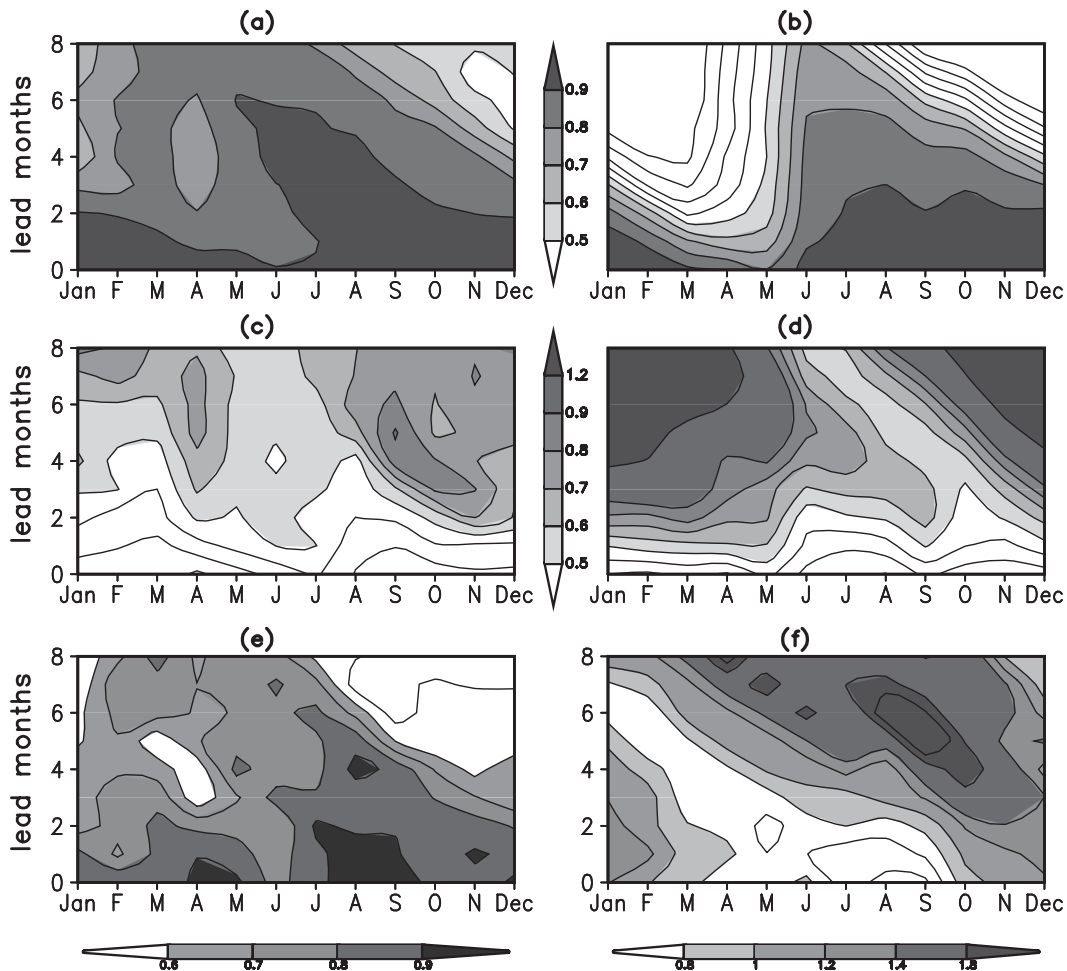


FIG. 2. (a) ACC of CFS ensemble mean forecasts of the monthly mean Niño-3.4 SST over the period 1981–2005 as a function of IC month (x axis) and lead month (y axis). Niño-3.4 is defined as the spatial mean SST over  $5^{\circ}\text{S}$ – $5^{\circ}\text{N}$ ,  $170^{\circ}$ – $120^{\circ}\text{W}$ . (b) As in (a), but for the persistence forecast. (c) As in (a), but for RMSE for the CFS ensemble forecast, and (d) as in (c), but for persistence forecast. (e) As in (a), but for CFS mean forecasts of the monthly mean precipitation anomalies over the equatorial Pacific ( $10^{\circ}\text{S}$ – $5^{\circ}\text{N}$ ,  $170^{\circ}\text{E}$ – $110^{\circ}\text{W}$ ). (f) As in (c), but for monthly mean precipitation anomalies over the equatorial Pacific.

at all leads, S/N, a measure of the spread, drops off by a factor of  $\sim 2.7$  (from 6.1 to 2.3), largely due to wider spread during cold events.

Third, in Fig. 5 we examine CFS's ability in forecasting the monthly Niño-3.4 SST anomalies during 1982 (open circles) and 1997 (open squares) events for four different ICs. These four ICs represent the predictions of the onset, intensification, peak amplitude, and decline or the transition phases of El Niño, respectively. For January ICs, the CFS predicts the warming tendency for both events but the amplitude is underestimated. In terms of both amplitude and timing, the 1997 event is best forecast with April ICs while the subsequent forecast with July and October ICs overestimates the strength, and even failed to predict the sudden phase transition to La Niña (a drop of  $\sim 1.5^{\circ}\text{C}$  during May–June of 1998;

Fig. 5d). For the 1982 event, however, the hindcasts with all ICs agree with the observations only for the first 2–4 months and thereafter the amplitude drifts by  $1^{\circ}$ – $2^{\circ}\text{C}$ .

Finally, we analyzed CFS's skill in forecasting different types of El Niño (Figs. 3b, 5). Observations indicate that the SST maximum for cold tongue events is over the eastern Pacific or Niño-3 region ( $5^{\circ}\text{S}$ – $5^{\circ}\text{N}$ ,  $90^{\circ}$ – $150^{\circ}\text{W}$ ), and that for warm pool events the maximum lies over the west-central Pacific or Niño-4 region ( $5^{\circ}\text{S}$ – $5^{\circ}\text{N}$ ,  $160^{\circ}\text{E}$ – $150^{\circ}\text{W}$ ). Therefore, the skill levels in hindcasting SST anomalies over Niño-3 and Niño-4 regions are examined. Owing to the role of wave-induced thermocline displacements influencing SST through vertical advection even at 6-month lead time, the ACC remains high (0.9) for the Niño-3 region and other skill measures are as good as that over the Niño-3.4 region and, hence, are

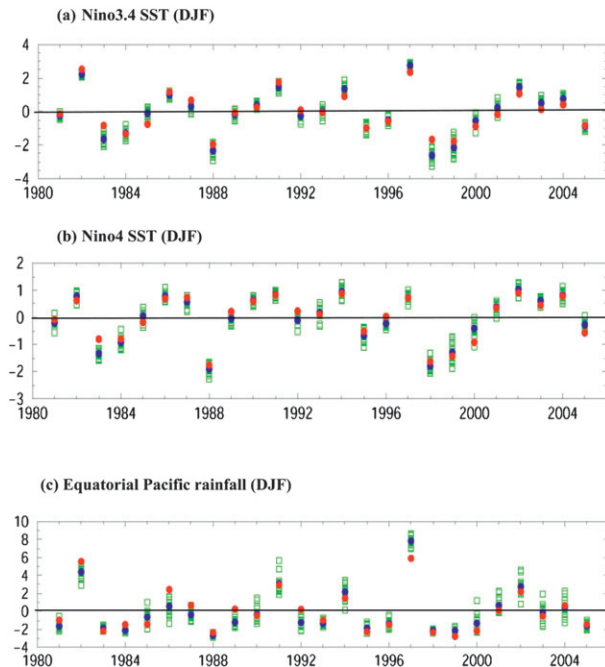


FIG. 3. (a)–(c) Temporal evolution of DJF SST anomalies ( $^{\circ}\text{C}$ ) hindcast by CFS at 0-month lead time. Ensemble mean (blue), all 15 individual members (green), and observations (red) are shown for two regions: (a) Niño-3.4 ( $5^{\circ}\text{S}$ – $5^{\circ}\text{N}$ ,  $190^{\circ}\text{E}$ – $120^{\circ}\text{W}$ ) and (b) Niño-4 ( $5^{\circ}\text{S}$ – $5^{\circ}\text{N}$ ,  $160^{\circ}\text{E}$ – $150^{\circ}\text{W}$ ). (c) As in (a), but for equatorial Pacific rainfall anomalies ( $\text{mm day}^{-1}$ ) averaged over  $10^{\circ}\text{S}$ – $5^{\circ}\text{N}$ ,  $170^{\circ}\text{E}$ – $110^{\circ}\text{W}$ .

not discussed further. At lag 0 over the Niño-4 region, local warming during the boreal winters of 1990/91, 1994/95, 2002/03, and 2004/05 are forecasted with a small spread (Fig. 3b). A particular aspect of the forecast is that the prolonged El Niño episode of 1991–95 is observed only over the Niño-4 region rather than over Niño-3.4 (Fig. 3a). As with strong events, we examined CFS's ability to forecast the evolution of Niño-4 SST anomalies during relatively weak events (1994/95 and 2002/03) for four different ICs (Fig. 6). For both events, the forecasts initialized in October show good agreement with the observations (in terms of amplitude and timing), including the termination phase, but the forecast performed with July ICs is rather poor. An examination for the entire period (Table 2) suggests that predictions of SST anomalies over both the Niño-3 and Niño-4 regions are comparable to those over Niño-3.4 for most leads.

In summary, CFS's skill is higher for forecasting stronger and persisting El Niño events that are primarily due to thermocline displacements. When seasonally stratified, predictions of winter and autumn seasonal SST anomalies have higher skill. However, forecasting weaker El Niño events is limited to 0–2-month leads.

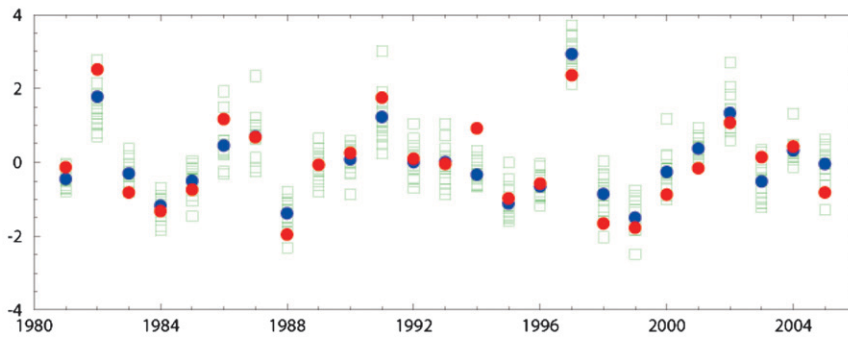
### b. Precipitation along the equatorial Pacific

The overall skill measures for precipitation forecasts along the equatorial Pacific ( $10^{\circ}\text{S}$ – $5^{\circ}\text{N}$ ,  $170^{\circ}\text{E}$ – $110^{\circ}\text{W}$ ) are shown in Figs. 2e,f and Table 1. High values of ACC ( $>0.7$ ) with less RMSE are along the diagonal representing the fall and winter seasons. For short lead times (0–2 months) only, predicting spring and summer rainfall is skillful, and similar to SST, forecasting precipitation anomalies during ENSO phase transition is difficult. Van Oldenborgh et al. (2005b) examined the skill of two versions of the ECMWF seasonal prediction system (S1 and S2) and noted that in both versions ACC is  $>0.7$  when predicting equatorial Pacific rainfall anomalies for all seasons except summer (see their Table 1). Despite differences in the physical parameterizations employed, the consistency between the CFS and ECMWF systems suggests that skill in predicting large-scale precipitation anomalies may be model independent.

Encouraged by the skill in forecasting aspects of El Niño-related SST anomalies in individual years, we turn our attention to precipitation skill along the equatorial Pacific at 0-month lead for the DJF season (Fig. 3c). While the ensemble mean follows the observed, the spread is larger, yielding an S/N of about 4.2, and this skill is considerably less than that for Niño-3.4 SST (Table 1a). Other limitations include excess rainfall during the winter of 1997/98, and the failure to capture the above normal rainfall during the winter of 1986/87. In addition, during cold phases of 1983/84 and 1998/99 (Fig. 3a), the precipitation forecast is weaker than observed (Fig. 3c) despite predicting stronger SST anomalies compared to the observations. SST anomalies translating into rainfall anomalies depend on the physical parameterizations employed, particularly convective schemes. Further, the SST–rainfall relationship is also not local, and rainfall anomalies can be influenced by circulation anomalies forced by rainfall at other locations.

Finally, to depict coherency among variables responsible for ocean–atmosphere interactions, lagged correlations between the DJF Niño-3.4 SST and SST (contours), rainfall (shaded), and 850-hPa wind (vector) anomalies at 0-month lead and spanning the 24-month period (entire life cycle of ENSO) are shown in Fig. 7b. Similar results from the observations are also shown in Fig. 7a. In CFS and at both leads, the onset, development, mature, and decay stages of El Niño, as well as the development of cold SST and negative precipitation anomalies over the Maritime Continent ( $120^{\circ}$ – $150^{\circ}\text{E}$ ), together with low-level divergence corresponding to an anomalous Walker circulation, are in good agreement with observations. Most of these salient features noted at 0-month lead are readily apparent even at 6-month lead (Fig. 4b). To the

(a) Niño-3.4 SST (DJF) – six month lead



(b)

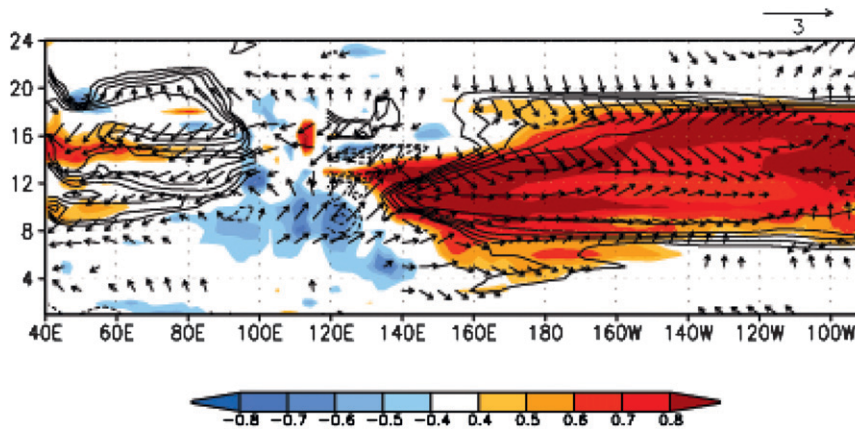


FIG. 4. (a) Temporal evolution of DJF average Niño-3.4 ( $5^{\circ}\text{S}$ – $5^{\circ}\text{N}$ ,  $190^{\circ}\text{E}$ – $120^{\circ}\text{W}$ ) SST anomalies ( $^{\circ}\text{C}$ ) hindcast by CFS at 6-month lead time for the ensemble mean (blue), all 15 individual members (green), and the observations (red). (b) Lagged correlations of SST (contours), rainfall (shaded), and 850-hPa wind averaged in  $3^{\circ}\text{S}$ – $3^{\circ}\text{N}$  with winter (DJF) Niño-3.4 SST index from the CFS ensemble mean 6-month lead forecast. Results are shown for a 2-yr period representing the entire life cycle of ENSO.

west of this center of divergence, easterly wind anomalies cover the entire equatorial Indian Ocean, and their influence on local ocean dynamics is explained next.

### c. Teleconnection to the TIO

Figure 7d shows lagged correlations between DJF Niño-3.4 time series and SSH (shaded) and SST (contours) averaged over ( $8^{\circ}$ – $12^{\circ}\text{S}$ ) the TIO from the observations, and the corresponding results from the 0-lead CFS forecast, are shown in Fig. 7e. Starting from May–June of year 0, upwelling-favorable winds off the Java–Sumatra coasts (Figs. 7a–c;  $80^{\circ}$ – $100^{\circ}\text{E}$ ) promote negative SSH values (i.e., shallow thermocline anomalies; Fig. 7e) and subsequent local SST cooling attains a maximum in fall (Figs. 7a–c). The wind stress curl associated with the easterly wind anomalies forces downwelling oceanic

Rossby waves, and the westward-tilted structures in the SSH and SST anomalies with respect to time (Figs. 6d,e) support that interpretation. These Rossby waves advect warm water and act to deepen the thermocline as they cross the ocean basin (Xie et al. 2002). The maximum perturbations to SSH (i.e., deepened thermocline) and SST are noted over SWIO during boreal spring of year +1. The warm SST anomalies persist for about 10–12 months primarily due to the presence of the shallow-mean thermocline and passage of oceanic Rossby waves. Other studies (e.g., Murtugudde and Busalacchi 1999; Shinoda et al. 2004) suggest the importance of evaporative cooling and solar radiation in contributing to SST anomalies over SWIO. The good skill in low-level wind (Fig. 4b) provides indirect evidence for evaporative cooling. In summary, CFS captures the teleconnection



TABLE 1. Values of ACC and S/N estimated for regional SST time series for four standard seasons, and for 0–6-month-lead forecasts.

| (a) Niño-3.4 region |      |     |      |     |       |     |      |     |
|---------------------|------|-----|------|-----|-------|-----|------|-----|
| Lead<br>(months)    | DJF  |     | MAM  |     | JJA   |     | SON  |     |
|                     | ACC  | S/N | ACC  | S/N | ACC   | S/N | ACC  | S/N |
| 0                   | 0.96 | 6.1 | 0.95 | 4.8 | 0.92  | 3.2 | 0.96 | 3.7 |
| 1                   | 0.92 | 5.2 | 0.91 | 3.0 | 0.82  | 2.6 | 0.93 | 3.2 |
| 2                   | 0.92 | 4.5 | 0.85 | 2.9 | 0.88  | 2.2 | 0.92 | 3.3 |
| 3                   | 0.94 | 3.6 | 0.84 | 2.9 | 0.82  | 2.0 | 0.88 | 2.5 |
| 4                   | 0.91 | 3.2 | 0.84 | 2.9 | 0.68  | 1.4 | 0.76 | 2.2 |
| 5                   | 0.91 | 2.8 | 0.81 | 2.9 | 0.50  | 1.5 | 0.85 | 2.0 |
| 6                   | 0.89 | 2.3 | 0.83 | 2.5 | 0.53  | 1.8 | 0.79 | 2.0 |
| (b) SWIO region     |      |     |      |     |       |     |      |     |
| Lead<br>(months)    | DJF  |     | MAM  |     | JJA   |     | SON  |     |
|                     | ACC  | S/N | ACC  | S/N | ACC   | S/N | ACC  | S/N |
| 0                   | 0.85 | 1.7 | 0.92 | 1.8 | 0.64  | 1.7 | 0.73 | 1.9 |
| 1                   | 0.84 | 1.7 | 0.87 | 1.6 | 0.57  | 1.2 | 0.60 | 1.3 |
| 2                   | 0.85 | 1.5 | 0.84 | 1.4 | 0.52  | 1.1 | 0.47 | 1.3 |
| 3                   | 0.82 | 1.4 | 0.85 | 1.5 | 0.50  | 0.9 | 0.42 | 1.1 |
| 4                   | 0.81 | 1.3 | 0.83 | 1.4 | 0.58  | 1.2 | 0.27 | 1.1 |
| 5                   | 0.75 | 1.1 | 0.85 | 1.5 | 0.57  | 1.0 | 0.13 | 1.1 |
| 6                   | 0.71 | 1.1 | 0.83 | 1.4 | 0.67  | 1.0 | 0.10 | 0.8 |
| (c) EEIO region     |      |     |      |     |       |     |      |     |
| Lead<br>(months)    | DJF  |     | MAM  |     | JJA   |     | SON  |     |
|                     | ACC  | S/N | ACC  | S/N | ACC   | S/N | ACC  | S/N |
| 0                   | 0.76 | 1.2 | 0.87 | 1.3 | 0.80  | 1.5 | 0.89 | 1.2 |
| 1                   | 0.61 | 1.0 | 0.80 | 1.0 | 0.73  | 1.3 | 0.76 | 1.0 |
| 2                   | 0.40 | 1.0 | 0.75 | 1.0 | 0.18  | 0.9 | 0.59 | 1.0 |
| 3                   | 0.29 | 1.0 | 0.77 | 1.0 | 0.03  | 0.7 | 0.71 | 1.0 |
| 4                   | 0.46 | 0.9 | 0.71 | 0.8 | -0.04 | 0.4 | 0.51 | 0.9 |
| 5                   | 0.48 | 0.9 | 0.67 | 0.9 | -0.3  | 0.5 | 0.18 | 0.9 |
| 6                   | 0.38 | 0.8 | 0.72 | 0.9 | -0.1  | 0.5 | 0.04 | 0.8 |

from the tropical Pacific to TIO, and also the essential mechanisms responsible for the anomalous conditions in the TIO.

Encouraged by the above results, we examined the deterministic skill scores over both SWIO (15°S–0°, 55°E–75°E) and EEIO (10°S–0°, 90°–110°E). Observations indicate the SST anomalies peak during spring of year +1 over SWIO and during boreal fall over EEIO. For SWIO, CFS hindcasts initialized during June–July of year 0 onward depict higher ACC and lower RMSE (Figs. 8a,b) than are found with the persistence method (Figs. 8b–d). In contrast, over EEIO the ensemble mean barely does better than persistence even at shorter leads (Figs. 8e,f). To test the model’s ability in forecasting one of the strongest IODZM events during 1997 and the subsequent warming over SWIO in spring of 1998, ensemble mean hindcasts at various leads are shown (Fig. 9). For IODZM (Fig. 9b), the model is successful only at 0-month lead and fails to forecast even the

cooling tendency at longer leads. In contrast, the progression and the amplitude of SWIO (Fig. 9a) warming are closer to the observations, even at 3–6-month lead time. In addition, the basin-wide warming covering the EEIO during the spring of year +1 is forecast at longer leads.

Finally, Tables 1b,c summarize the CFS skill in forecasting SWIO and EEIO SST anomalies at various leads and for all seasons. For winter and the following spring over SWIO, the skill is relatively higher for longer leads but the S/N never reaches 2.0. But over EEIO, except for the 0-month lead, the spread among the ensemble members (i.e., the noise) is comparable to the spread of the ensemble mean (i.e., the signal). An examination of all strong IODZM events during the period 1982–2005 indicates that while ACC is about 0.9 at 0-month lead, spread masks the S/N (Table 1c). The limitations in the SST forecast are reflected in the low skill for local precipitation anomalies (not shown). One factor is that even during strong events, the observed SST anomalies over SWIO and EEIO are around 0.8°C (Fig. 9a) and 1.4°C (Fig. 9b), respectively. Thus, despite a clear influence of ocean dynamics, predicting these SST anomalies may require, among other things, a better representation of the monsoon, oceanic processes and higher resolution to represent upwelling off the Java–Sumatra islands.

#### d. SST over the tropical Atlantic region

SST anomalies over the tropical Atlantic during boreal summer favor the development and intensification of hurricanes, and hence CFS’s ability in hindcasting SST over the region (10°–20°N, 20°–80°W) is examined (Figs. 8i–l). The ensemble mean forecast outperforms persistence particularly for ICs ranging from May to July. With low RMSEs, forecasting the SST during the hurricane season is well represented in CFS, unlike the moderate skill in ECMWF S3 (Stockdale et al. 2011). However, unlike the skill over Niño-3.4 (Fig. 2a), over the tropical Atlantic the ACC skill (>0.7) lasts only for a few lead months (2–4 months).

#### e. Precipitation over the USAPI

Figure 10 shows the rainfall forecast over the western Pacific islands (5°–15°N, 125°–165°E). The left (right) panels are results for 0-month (6 month) lead time for standard seasons of summer (Figs. 10a,b), fall (Figs. 10c,d), winter (Figs. 10e,f), and spring (Figs. 10g,h). Note that the precipitation variance among the ensemble members is high here in all seasons (Fig. 1). Observations (red circles) indicate that during strong El Niño years (e.g., 1982–83, 1991–92, and 1997–98), dryness (or below normal rainfall) persists from winter of year 0 to summer of year +1. Quite remarkably, the

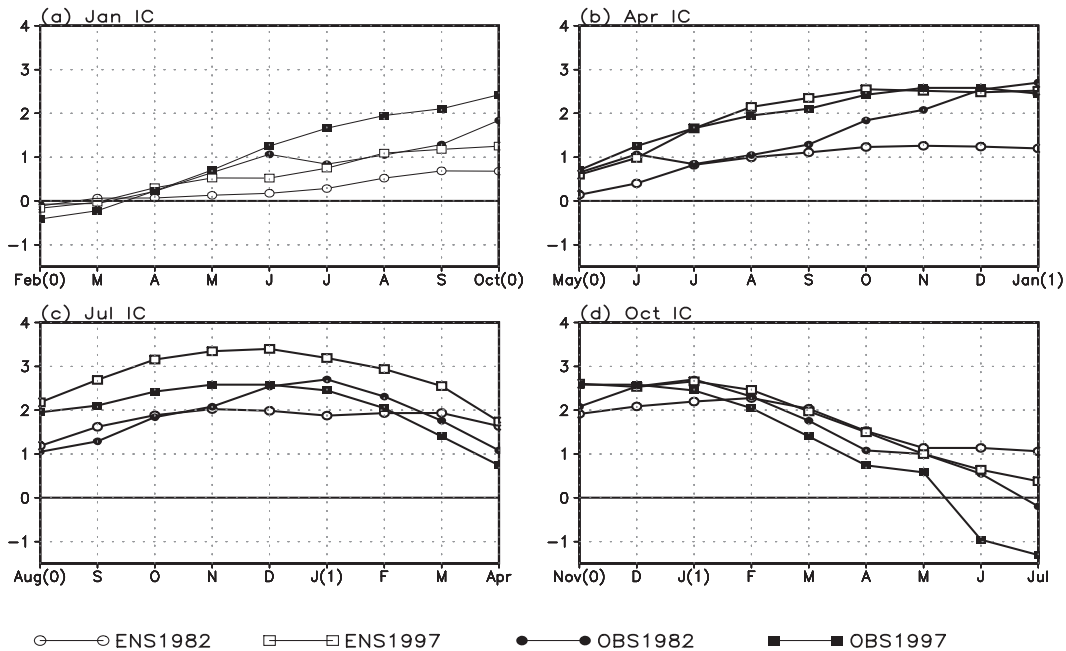


FIG. 5. Monthly anomalous Niño-3.4 SST ( $^{\circ}\text{C}$ ) index for the 1982 and 1997 El Niño events for predictions starting from (a) January, (b) April, (c) July, and (d) October ICs. Here, OBS indicates observation and ENS stands for ensemble mean.

CFS ensemble-mean forecast (blue circles) captures this drying tendency from 6-month lead time except for summer of year +1. Barring the two strong El Niño events of 1982/83 and 1997/98, the spread among the ensemble members is large but the sign of the anomalies is well captured. For 6-month-lead forecasts of JJA rainfall, the predicted sign is wrong in many years. While correlations between rainfall anomalies over the western Pacific and Niño-3.4 SST anomalies are negative for most of the year, they are rather positive during July–August. Thus, the difficulty in capturing this seasonally varying teleconnection may well be a factor in the low skill scores during summer. Table 3a lists the statistics at various leads and for all seasons. The ACC and S/N are high for winter and spring, but both drop off to low values for summer and fall (Table 3a). A possible interpretation is that large-amplitude swings in precipitation occur during winter (Fig. 10e) and, hence, are more predictable.

Figure 11 shows the results for the South Pacific islands ( $10^{\circ}$ – $30^{\circ}\text{S}$ ,  $160^{\circ}$ – $200^{\circ}\text{E}$ ), and the skill statistics is summarized in Table 3b. In this region too, largest anomalies in precipitation are observed during ENSO winters (Figs. 11a,b) but the dryness starts during the summer of year 0 and persists until the following spring. Interestingly, CFS correctly captures both the phase and amplitude of the dryness at longer lead times. However, for any given season ACC and S/N do not exceed 0.7 and 2.0, respectively. Compared to other seasons, forecasting

rainfall anomalies during summer is less skillful (Table 3b) since the ENSO teleconnection is weaker.

Another region of interest is the Hawaiian Archipelago ( $15^{\circ}$ – $30^{\circ}\text{N}$ ,  $170^{\circ}$ – $140^{\circ}\text{W}$ ). The precipitation forecasts are shown in Fig. 12 and the statistics are summarized in Table 3c. For the islands situated over the Northern Hemisphere, western Pacific, and Hawaii, the dryness attains a maximum in winter of year 0 and continues into the spring of year +1, and CFS has skill in forecasting them. However, the spread among the members is indeed large even during the 1982–83 and 1997–98 El Niño years (Fig. 12) resulting in a low S/N (Table 3c). Further, the analysis of ensemble mean SD and spread (table not shown) reveals that they are almost identical, implying limitations in precipitation forecasts over the Hawaiian region. An analysis of ACC and RMSE for the USAPI regions for all leads and ICs (not shown) confirms the above results. Briefly, for both the western Pacific and South Pacific regions high (low) ACC (RMSE) values at 5–6-month lead lie along the diagonal that represents the winter and spring rainfall. However, rainfall anomalies over the Hawaiian Islands appear to be least predictable at longer leads. From Figs. 10–12, it is encouraging to note that observed anomalies (red dots) generally lie within the envelope of possible model solutions (green dots), and there are few instances of outliers. On the other hand, in all three regions the interannual variability in the envelope of the ensemble spread is large enough

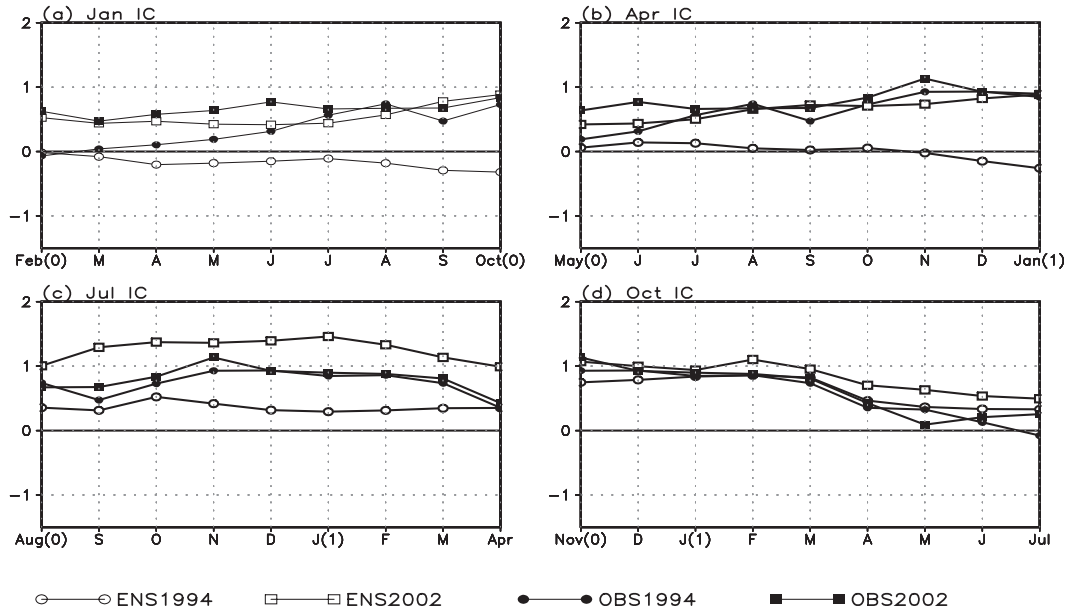


FIG. 6. Monthly anomalous Niño-4 SST ( $^{\circ}\text{C}$ ) index for the 1994 and 2002 El Niño events for the predictions starting from (a) January, (b) April, (c) July, and (d) October ICs. Here, OBS indicates observation and ENS stands for ensemble mean.

(1.0–5.0 mm day<sup>-1</sup>). In addition, the ratio between SD and ensemble spread for the regional rainfall anomalies is not high (not shown), suggesting model limitations. One area of improvement is to perform forecasts with a higher horizontal resolution to capture the orographically induced rainfall. Another approach is to perform statistical downscaling.

**4. Assessment of different aspects of forecasts**

In this section, ACC is compared and contrasted with HSS and RPSS to assess different aspects associated with forecasts that also rely on the spread information inherent in the ensembles. Our working hypothesis is that forecast assessments based on ACC alone are not sufficient enough within the context of decision making, and alternate measures for assessing probabilistic forecasts are also needed. The comparison is first made over the global tropics (section 4a) and then over selected regions (section 4b). One expects some correspondence between various skill measures; for example, an ACC value of 0.5 for a deterministic forecast is comparable to about 30%–35% of HSS for the categorical forecast, and 15%–20% of RPSS (Kumar 2009) for the probabilistic forecast. However, it may not be true if the spread among ensemble members (upon which probabilistic forecasts rely) has biases compared to the observations. For example, ACC as a measure of skill for deterministic forecasts does not depend on the spread among ensemble

members and, therefore, may be not be sensitive to errors in such; while an analysis-based probabilistic measure (e.g., RPSS) will be sensitive to those errors.

*a. Assessment of errors over the tropics*

Figure 13 shows spatial maps of ACC, HSS, and RPSS for SST and precipitation forecasts at 0-month lead for

TABLE 2. As in Table 1, but for SST anomalies.

| (a) Niño-3 region |      |     |     |     |     |     |      |     |
|-------------------|------|-----|-----|-----|-----|-----|------|-----|
| Lead (months)     | DJF  |     | MAM |     | JJA |     | SON  |     |
|                   | ACC  | S/N | ACC | S/N | ACC | S/N | ACC  | S/N |
| 0                 | 0.95 | 6.0 | 0.9 | 4.2 | 0.9 | 3.5 | 0.95 | 3.8 |
| 1                 | 0.92 | 5.5 | 0.9 | 2.7 | 0.9 | 2.7 | 0.9  | 2.9 |
| 2                 | 0.92 | 4.5 | 0.8 | 2.6 | 0.8 | 2.2 | 0.9  | 2.9 |
| 3                 | 0.90 | 3.4 | 0.8 | 2.8 | 0.8 | 2.0 | 0.9  | 2.3 |
| 4                 | 0.90 | 2.9 | 0.8 | 2.7 | 0.7 | 1.2 | 0.8  | 2.0 |
| 5                 | 0.89 | 2.6 | 0.7 | 2.9 | 0.6 | 1.3 | 0.8  | 1.8 |
| 6                 | 0.88 | 2.0 | 0.8 | 2.4 | 0.6 | 1.6 | 0.8  | 1.9 |

| (b) Niño-4 region |      |     |     |     |     |     |      |     |
|-------------------|------|-----|-----|-----|-----|-----|------|-----|
| Lead (months)     | DJF  |     | MAM |     | JJA |     | SON  |     |
|                   | ACC  | S/N | ACC | S/N | ACC | S/N | ACC  | S/N |
| 0                 | 0.96 | 5.1 | 0.9 | 4.7 | 0.9 | 3.6 | 0.95 | 3.6 |
| 1                 | 0.92 | 4.2 | 0.9 | 3.1 | 0.9 | 2.6 | 0.9  | 3.4 |
| 2                 | 0.91 | 3.5 | 0.9 | 2.9 | 0.9 | 2.3 | 0.9  | 3.4 |
| 3                 | 0.87 | 2.9 | 0.9 | 3.0 | 0.9 | 2.1 | 0.8  | 2.9 |
| 4                 | 0.83 | 2.9 | 0.9 | 2.8 | 0.8 | 1.6 | 0.7  | 2.2 |
| 5                 | 0.80 | 2.9 | 0.9 | 2.7 | 0.6 | 1.7 | 0.8  | 2.1 |
| 6                 | 0.78 | 2.3 | 0.9 | 2.4 | 0.7 | 2.1 | 0.8  | 2.1 |

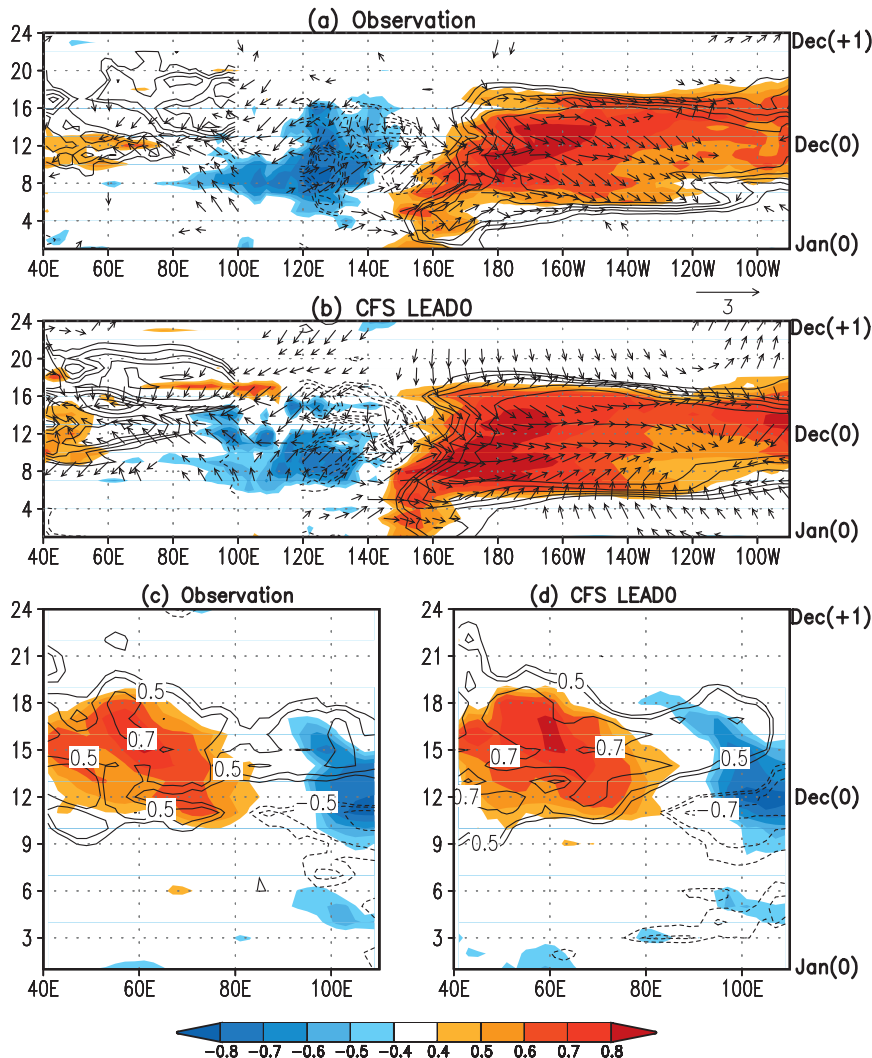


FIG. 7. (a) Lagged correlations of SST (contours), and rainfall (shaded), and 850-hPa-wind averaged over  $3^{\circ}\text{S}$ – $3^{\circ}\text{N}$  with a winter (DJF) Niño-3.4 SST index from the observations. (b) As in (a), but from the CFS ensemble mean 0-month lead forecast. Results are shown for a 2-yr period representing the entire life cycle of ENSO. (c) Lagged correlations of SST (contours) and SSH (shaded) averaged over  $8^{\circ}$ – $12^{\circ}\text{S}$  with the winter Niño-3.4 SST index from observations. (d) As in (c), but from the CFS ensemble mean 0-month lead forecast. Positive (negative) SST values are shown as solid (dashed) contours with an interval 0.1.

two seasons (spring and winter). For the sake of conciseness, figures from other seasons and other leads are not shown but the results are discussed briefly. Over the equatorial Pacific, all three of the skill measures agree quite well, enhancing our confidence in CFS forecasts. The exceptions include (i) negative RPSS values for precipitation over the far-eastern equatorial Pacific region during winter and (ii) the HSS and RPSS patterns being rather noisy, when compared to ACC patterns for rainfall in spring. Over SWIO, while ACC indicates high skill for both SST and rainfall, the coherency in HSS and RPSS is better captured for SST rather than for rainfall.

Over the USAPI, all three measures show a good degree of consistency with local maxima in their vicinities, but the consistency for higher skill scores is noticed over the western Pacific islands alone.

#### b. Regional indices

As before, we assess the scores for four SST indices (Fig. 14). The left panels in Fig. 14 are scatter diagrams between ACC and HSS, while the right panels are scatterplots between ACC and RPSS. From these plots, one can infer the merits and drawbacks associated with various aspects of the forecast information.



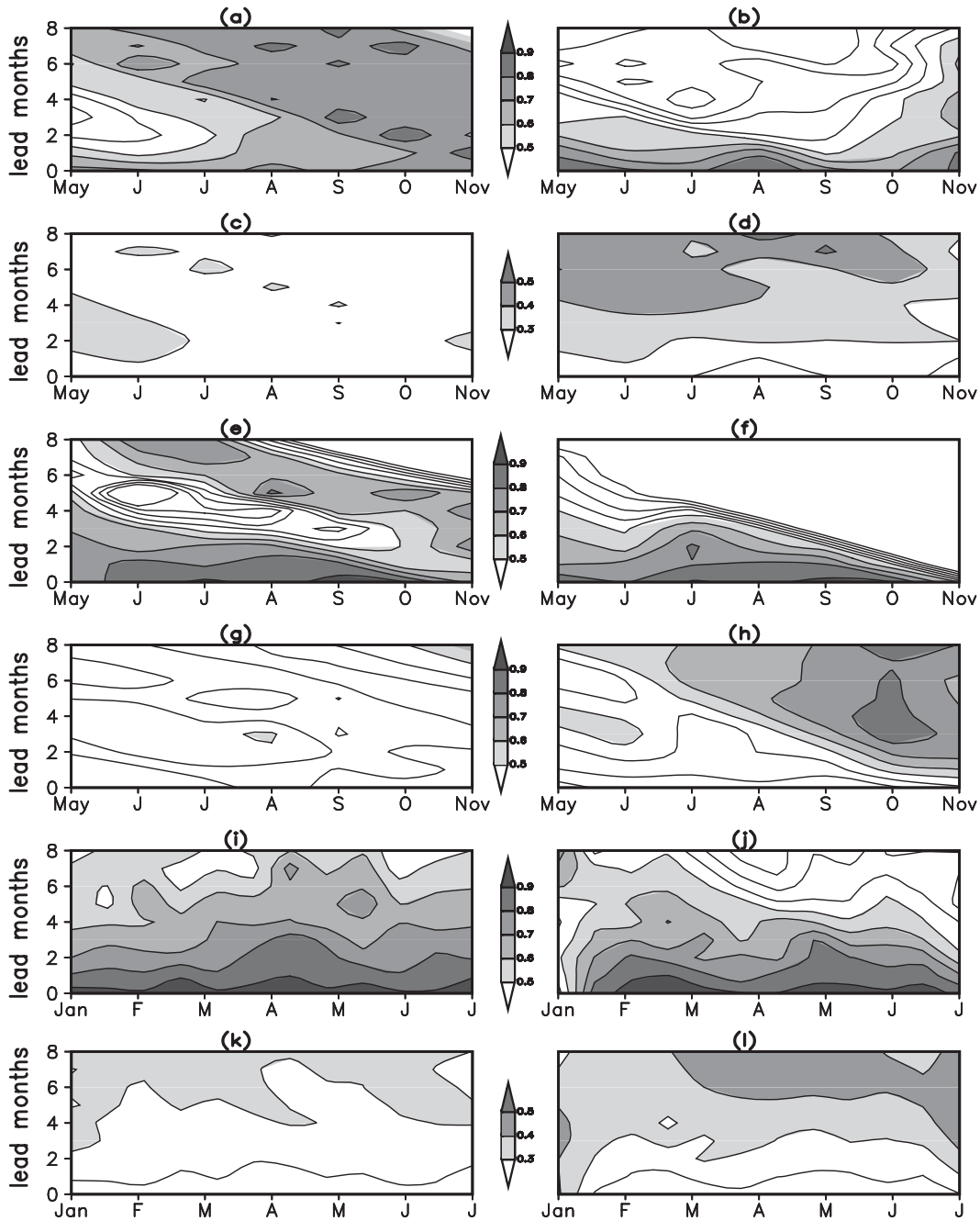


FIG. 8. (a) As in Fig. 2a, but for the SWIO SST index. (b) As in Fig. 2b, but for the SWIO SST index. (c),(d) As in Figs. 2c,d, but for the SWIO SST index. (e),(f) As in (a),(b), but for EEIO SST index. (g),(h) As in (c),(d), but for the EEIO SST index. (i),(j) As in (a),(b), but for the Atlantic SST index. (k),(l) As in (c),(d), but for Atlantic SST index. Please see Fig. 1 for regions used for averaging.

CFS demonstrates the highest confidence in predicting winter SST anomalies (Figs. 14a,b, open squares) over the Niño-3.4 region at all lead months with ACC upward of 0.85. High skill in deterministic forecasts as measured by ACC is also captured for categorical and probabilistic forecasts with high HSS (>50%) and RPSS

(>40%). This is consistent with the results discussed earlier (Fig. 2). The confidence in predicting the fall season is also high but limited to 0–4-month leads. Predicting spring and summer anomalies results in limited confidence at 0–1-month leads, and for other leads, even if ACC lies around 0.8, RPSS drops off to very low

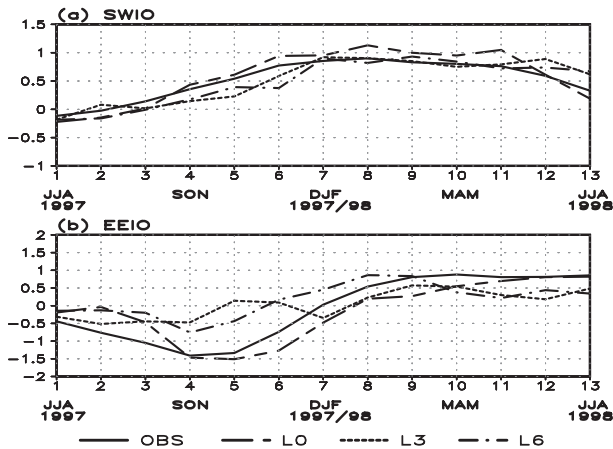


FIG. 9. The 3-month-average CFS ensemble mean SST ( $^{\circ}\text{C}$ ) forecast at 0- (dashed), 3- (dotted), and 6- (dash-dot) month leads over (a) SWIO and (b) EEIO. The starting period is summer (JJA) of 1997, the next period is July–September (JAS) of 1997, and so on. The corresponding observed SST is also shown (solid line).

values, sometimes even negative, indicating possible issues related to the spread among the ensemble members that influence the probabilistic forecasts. Therefore, forecasting the summer teleconnection features (e.g., ENSO–monsoon association) will be limited in CFS.

For the SST indices over the TIO, the confidence in predicting the winter and spring variations over SWIO (Figs. 14c,d) are high at leads up to 5 months. Watanabe and Jin (2003) and Annamalai et al. (2005a, 2007) noted that it is the winter and spring SST anomalies over SWIO that influence the regional and global climate anomalies. In the observations, summer and fall SST variations over SWIO are indeed small (Annamalai et al. 2003), and hence the models have limited predictability. In agreement with Wajsovicz (2005), our confidence in predicting IODZM SST anomalies during fall is the lowest (Figs. 14e,f).

We now examine the scatter diagrams for Atlantic SST anomalies between HSS and ACC (Fig. 14g) and between RPSS and ACC (Fig. 14h). Compared to other seasons, CFS demonstrates skill in predicting boreal fall SST anomalies (cross) with ACC ( $>0.85$ ), HSS ( $>40$ ), and RPSS ( $>10$ ), even though it is limited to 2-month lead. Except for 0-month leads, predicting SST anomalies in winter, spring, and summer has limited skill. The interpretation is that even if ACC lies around 0.5–0.7, RPSS drops off to lower values and occasionally negative values (particularly during the summer season).

The scatterplots over the USAPI are shown in Fig. 15. Over the western Pacific region, forecasting rainfall variations during winter is trustworthy for at least 0–3-month lead, followed by predictions for the spring season at leads of 0–1 month. For summer rainfall variations, while

ACC is greater than 0.6 and HSS is around 15%–25%, negative RPSS indicates that the forecast is not better than climatology. The model’s forecast for fall rainfall anomalies is least skillful. A point to note here is that for the same value of ACC ( $\sim 0.6$ ) for a 0–1-month lead forecast, RPSS is positive for spring but negative for summer, indicating the seasonal dependency in the forecast errors. For the South Pacific region, predicting rainfall variations during winter and spring appears realistic for leads of 0–4 months. Here also forecasting summer precipitation anomalies is not reliable. For the Hawaiian region, at shorter leads (0–1 month) and for all seasons except fall, convergence of all three scores suggests that different rainfall forecast information is useful. In summary, for regional precipitation forecasts over USAPI, ACC values greater than 0.7 and correspondingly high HSS and RPSS values occur particularly for the winter and spring seasons.

## 5. Real-time forecast assessment during 2006–09

Here, we present forecast skill for tropical SST (section 5a) and then rainfall over the USAPI (section 5b). Because of the limited forecast period, instead of seasonal anomalies, skill at the 0-, 3-, and 6-month lead forecasts for 3-month running mean anomalies are estimated.

### a. Tropical SST indices

Predictions of the 3-month average SST anomalies are shown over the Niño-3.4 (Fig. 16a), Niño-4 (Fig. 16b), SWIO (Fig. 16c), and EEIO (Fig. 16d) regions at two leads (0 and 3 months). Over the Niño-3.4 and Niño-4 regions, the moderate warm events of 2006 and 2009 are well predicted at 0-month lead, but at other leads, the predicted amplitude and phase are off target. For example, the observed peak warm SST anomalies during fall–early winter of 2006, particularly the early withdrawal of El Niño (phase transition), were not correctly predicted at 3-month lead. A similar problem is also noticed during the 2007/08 La Niña phase transition. While hindcasts of different types of El Niño demonstrated high skill at various lead times (Fig. 3), the real-time forecast skill of these events is modest. The skill measures of ACC and S/N shown in Table 3a for the Niño-3.4 region suggest a sharp degradation at 3-month lead and onward. This discrepancy is possibly due to low-amplitude short-duration ENSO events during this period (Wang et al. 2010).

An examination of the real-time prediction of SWIO SST anomalies (Fig. 16c) indicates that systematic errors noted in ENSO prediction (Fig. 16a) are also present here. As noted in hindcasts (Figs. 7, 8), the prediction of

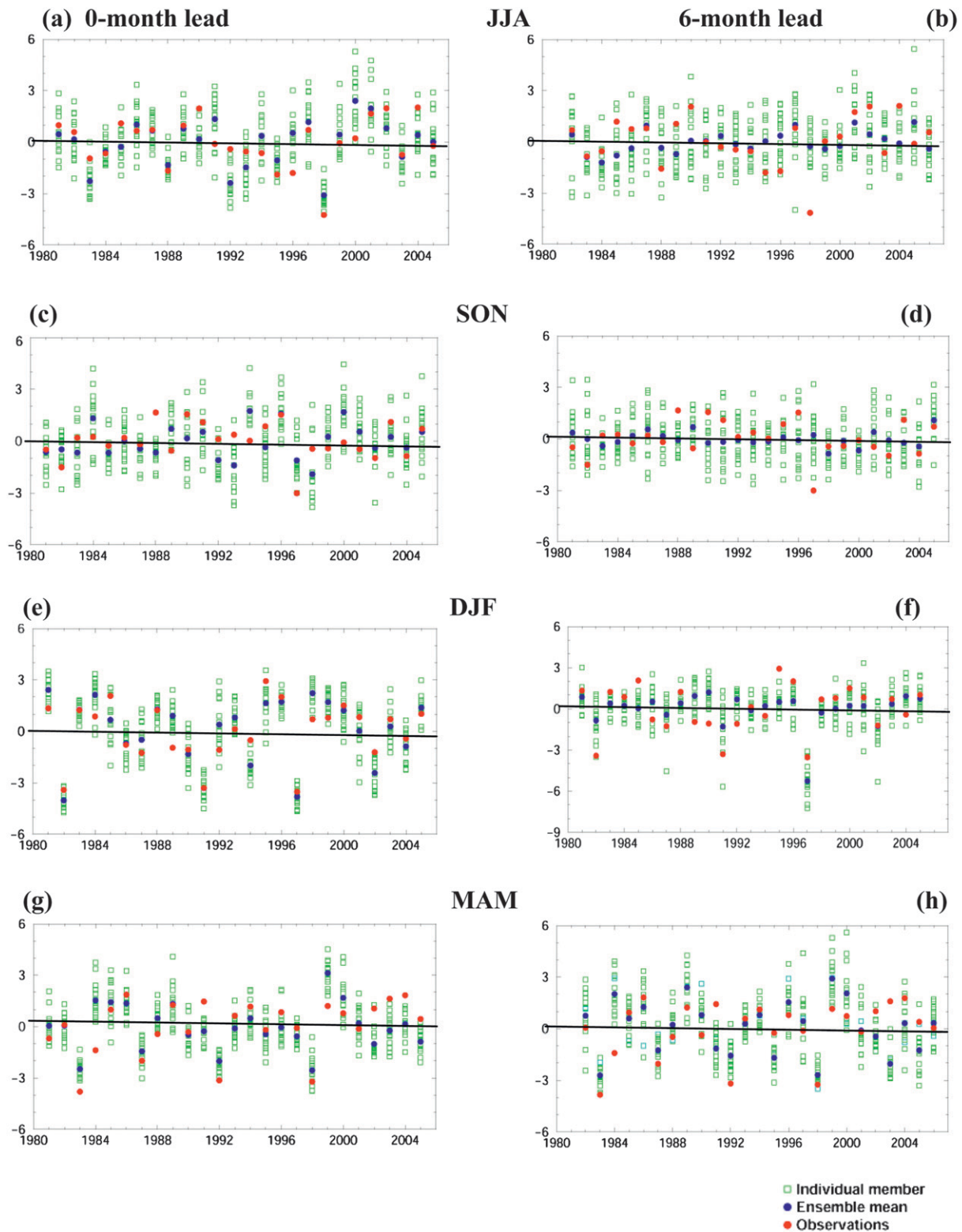


FIG. 10. Seasonal rainfall ( $\text{mm day}^{-1}$ ) forecast at (left) 0- and (right) 6-month lead times over the tropical west North Pacific region for the period 1981–2005. Observations (red), ensemble mean (blue), and all of the 15 individual members (green) are shown.

TABLE 3. As in Table 1, but for regional precipitation time series over the Pacific Islands.

| (a) Western Pacific region (5°–15°N, 125°–165°E) |      |     |      |     |      |     |       |     |
|--|------|-----|------|-----|------|-----|-------|-----|
| Lead (months)                                    | DJF  |     | MAM  |     | JJA  |     | SON   |     |
|  | ACC  | S/N | ACC  | S/N | ACC  | S/N | ACC   | S/N |
| 0  | 0.87 | 2.3 | 0.66 | 1.7 | 0.66 | 1.2 | 0.31  | 0.8 |
| 1  | 0.77 | 1.9 | 0.63 | 1.2 | 0.69 | 1.1 | −0.07 | 0.8 |
| 2  | 0.73 | 1.5 | 0.57 | 1.4 | 0.61 | 0.9 | −0.06 | 0.6 |
| 3  | 0.84 | 1.7 | 0.54 | 1.5 | 0.69 | 0.8 | −0.44 | 0.5 |
| 4  | 0.75 | 1.5 | 0.47 | 1.3 | 0.65 | 0.5 | 0.28  | 0.5 |
| 5  | 0.72 | 1.3 | 0.50 | 1.5 | 0.56 | 0.5 | −0.07 | 0.4 |
| 6  | 0.58 | 1.3 | 0.53 | 1.5 | 0.22 | 0.5 | −0.09 | 0.4 |
| (b) South Pacific region (10°–30°S, 160°E–160°W) |      |     |      |     |      |     |       |     |
| Lead (months)                                    | DJF  |     | MAM  |     | JJA  |     | SON   |     |
|  | ACC  | S/N | ACC  | S/N | ACC  | S/N | ACC   | S/N |
| 0  | 0.69 | 2.0 | 0.72 | 1.7 | 0.56 | 1.8 | 0.72  | 1.7 |
| 1  | 0.69 | 1.9 | 0.75 | 1.4 | 0.46 | 1.4 | 0.62  | 1.7 |
| 2  | 0.63 | 1.6 | 0.72 | 1.5 | 0.32 | 1.2 | 0.62  | 1.4 |
| 3  | 0.56 | 1.4 | 0.65 | 1.5 | 0.32 | 1.2 | 0.52  | 1.3 |
| 4  | 0.51 | 1.2 | 0.67 | 1.2 | 0.44 | 1.0 | 0.39  | 1.1 |
| 5  | 0.41 | 1.0 | 0.74 | 1.6 | 0.22 | 1.0 | 0.49  | 1.0 |
| 6  | 0.35 | 1.0 | 0.71 | 1.4 | 0.37 | 1.2 | 0.48  | 1.0 |
| (c) HI region (15°–30°N, 170°–140°W)             |      |     |      |     |      |     |       |     |
| Lead (months)                                    | DJF  |     | MAM  |     | JJA  |     | SON   |     |
|  | ACC  | S/N | ACC  | S/N | ACC  | S/N | ACC   | S/N |
| 0  | 0.62 | 1.1 | 0.69 | 1.5 | 0.57 | 1.4 | 0.49  | 0.9 |
| 1  | 0.69 | 1.0 | 0.44 | 1.3 | 0.69 | 1.1 | 0.44  | 1.0 |
| 2  | 0.60 | 0.9 | 0.52 | 1.3 | 0.62 | 1.1 | 0.32  | 0.9 |
| 3  | 0.57 | 0.9 | 0.49 | 1.1 | 0.64 | 1.1 | 0.22  | 0.8 |
| 4  | 0.34 | 0.7 | 0.46 | 1.2 | 0.46 | 0.8 | 0.39  | 0.7 |
| 5  | 0.27 | 0.6 | 0.34 | 1.3 | 0.55 | 0.9 | 0.12  | 0.6 |
| 6  | 0.14 | 0.6 | 0.49 | 1.0 | 0.61 | 0.9 | 0.34  | 0.7 |

the peak phase of IODZM during fall of 2006 is poor (Fig. 16d). Also, the model incorrectly predicts a very strong IODZM during the summer of 2008. The skill measures for SWIO and EEIO SST indices (Table 3a) indicate that the real-time prediction of the latter is very limited. For the forecast period 2005–08, Wang et al. (2010) examined the spatial distribution of ACC for SST and found that at 0-month lead values are high over the tropical Pacific, SWIO, and northern Atlantic.

### b. Precipitation indices

The skill of real-time precipitation forecasts over the equatorial central Pacific (Fig. 16e) and over the three regions of the USAPI (Figs. 16f–h), together with the skill measures (Table 3b), are examined. As for the hindcasts (Figs. 2, 3), there is generally a one-to-one correspondence in skill between SST and rainfall over the equatorial Pacific. Since there is a seasonal dependence in hindcast skill of regional rainfall (Table 2), a direct comparison with a 3-month average for real-time prediction

TABLE 4. As in Table 1, but for 3-month averages and for real-time forecasts for the period 2006–09.

| (a) SST time series                        |                 |     |               |     |      |     |
|--|-----------------|-----|---------------|-----|------|-----|
| Lead (months)                              | Niño-3.4        |     | SWIO          |     | EEIO |     |
|  | ACC             | S/N | ACC           | S/N | ACC  | S/N |
| 0  | 0.95            | 4.3 | 0.8           | 1.5 | 0.7  | 1.6 |
| 1  | 0.9             | 3.3 | 0.77          | 1.4 | 0.5  | 1.1 |
| 2  | 0.8             | 2.8 | 0.7           | 1.3 | 0.3  | 0.9 |
| 3  | 0.7             | 2.2 | 0.6           | 1.2 | 0.2  | 0.8 |
| 4  | 0.6             | 1.9 | 0.56          | 1.0 | 0.3  | 0.7 |
| 5  | 0.5             | 1.6 | 0.5           | 0.9 | 0.2  | 0.6 |
| 6  | 0.4             | 1.4 | 0.45          | 0.8 | 0.1  | 0.5 |
| (b) Precipitation over the Pacific Islands |                 |     |               |     |      |     |
| Lead (months)                              | Western Pacific |     | South Pacific |     | HI   |     |
|  | ACC             | S/N | ACC           | S/N | ACC  | S/N |
| 0  | 0.3             | 0.9 | 0.6           | 1.5 | 0.7  | 1.0 |
| 1  | 0.1             | 1.1 | 0.5           | 1.3 | 0.7  | 0.9 |
| 2  | 0.2             | 0.9 | 0.4           | 1.2 | 0.6  | 0.8 |
| 3  | 0.2             | 0.8 | 0.3           | 1.1 | 0.6  | 0.8 |
| 4  | 0.2             | 0.8 | 0.1           | 1.0 | 0.6  | 0.8 |
| 5  | 0.2             | 0.7 | 0.1           | 0.8 | 0.5  | 0.7 |
| 6  | 0.4             | 0.5 | 0.1           | 0.8 | 0.4  | 0.7 |

is not possible. Nevertheless, over the USAPI, the model's real-time forecast of precipitation over the Hawaiian Islands is better than for the other two regions. Over the South Pacific region, while CFS fails to predict negative (positive) rainfall anomalies during early months of 2006 (2007), the prediction of the anomalous conditions for 2008–09 is correct. However, prediction of rainfall variations over the tropical western Pacific (Fig. 16f; Table 4) is not encouraging compared to the high skill of the hindcasts noted earlier (Table 3a).

Compared to the high skill noted in the hindcasts (section 3), the modest skill in real-time forecasts needs attention. As a quantitative measure, for each of the SST and rainfall indices in Fig. 16 their respective standard deviation and ensemble spread are provided. Keeping in mind the short verification period, the ensemble spread is comparable to the standard deviation for all of the indices. In other words, the variance explained over the target regions is not strong enough.

## 6. Implications for dynamical seasonal prediction of precipitation

Both observational (Ropelewski and Halpert 1987, 1989) and modeling (e.g., Shukla 1998; Su and Neelin 2002) studies provide a guide to the expected climatic impacts of ENSO over the tropics. The fact that an accurate prediction of the tropical Pacific SST is a necessary condition for the successful prediction of rainfall



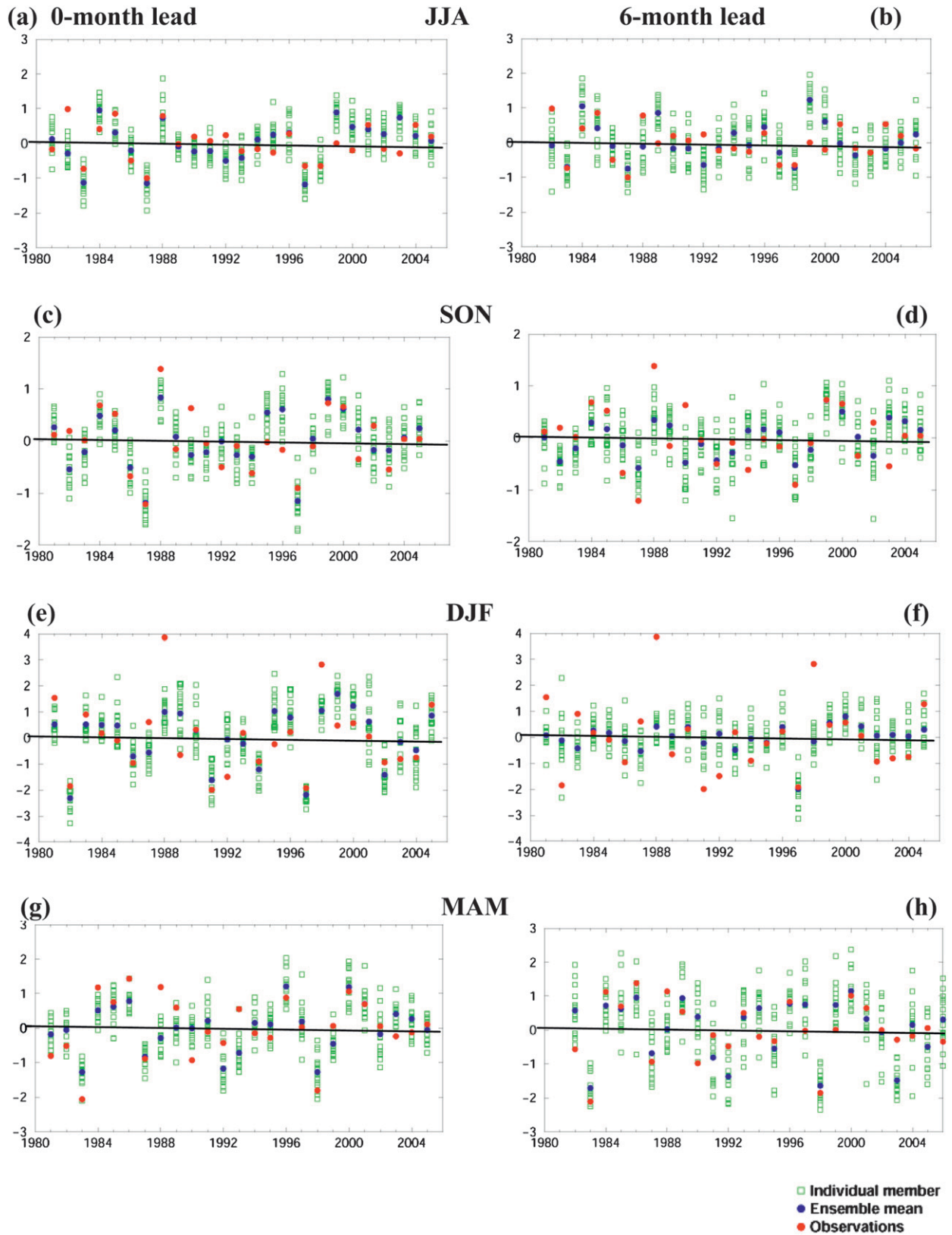


FIG. 11. As in Fig. 10, but for precipitation (mm day<sup>-1</sup>) over the South Pacific region.

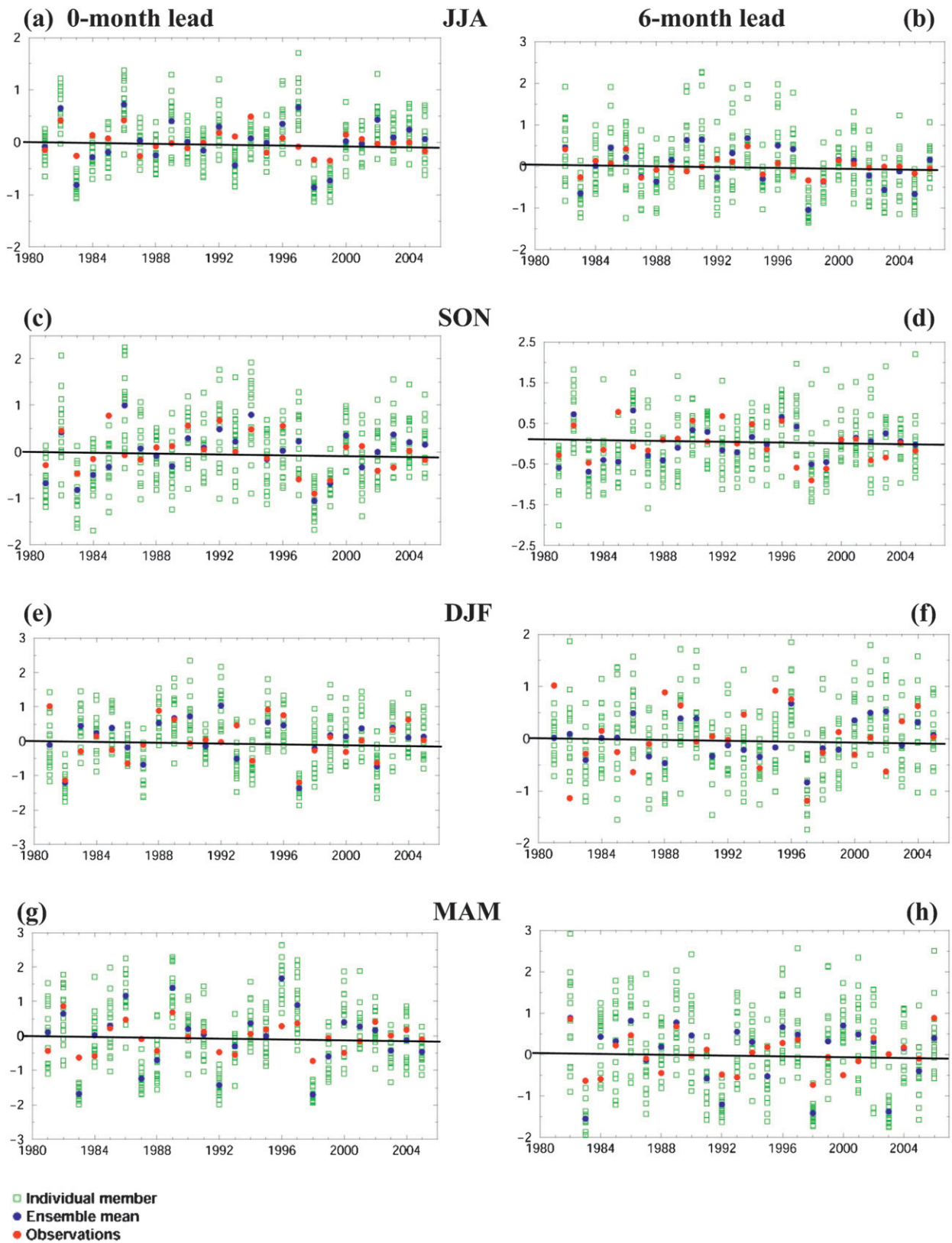


FIG. 12. As in Fig. 10, but for precipitation ( $\text{mm day}^{-1}$ ) the HI region.

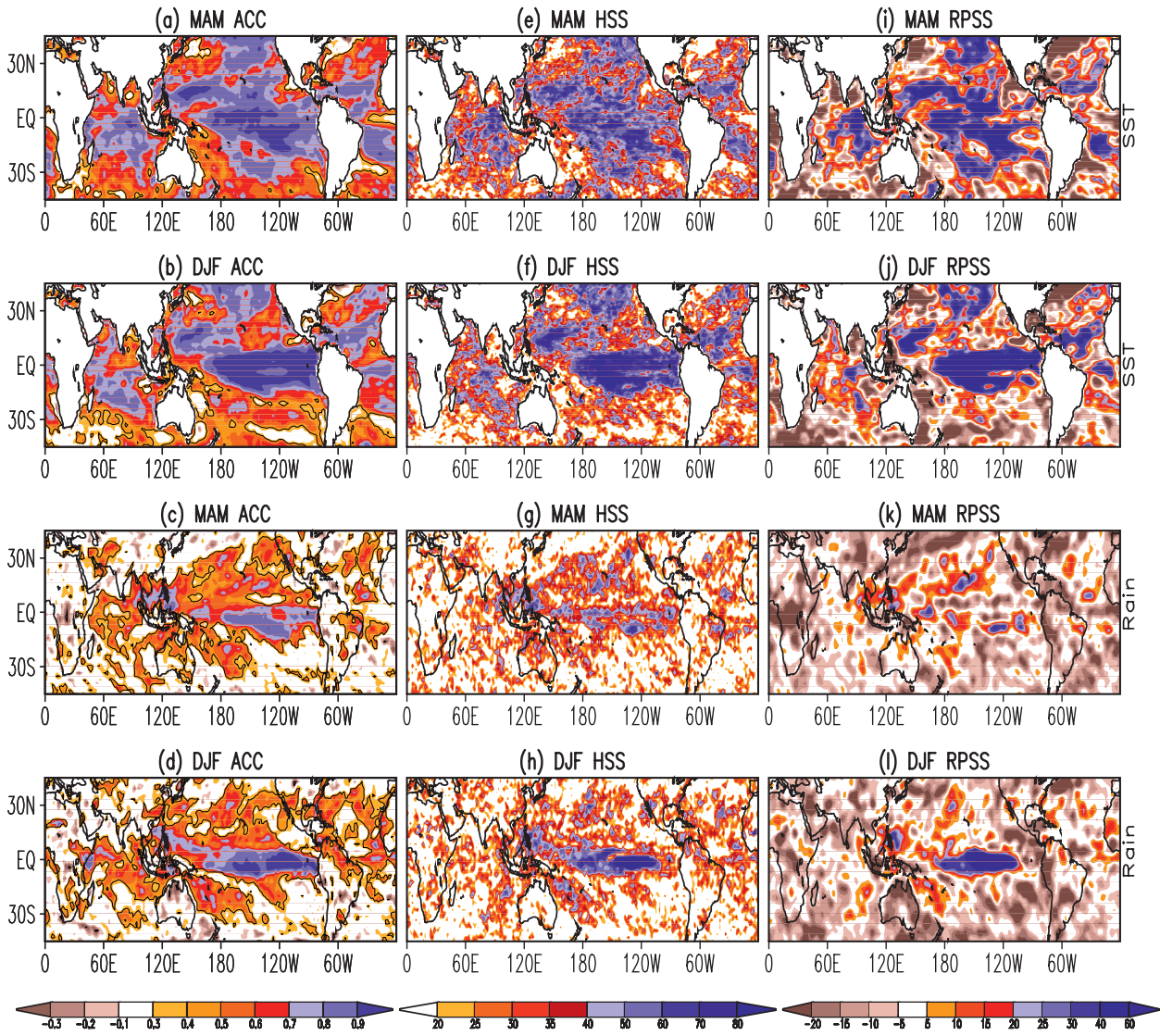


FIG. 13. (left) ACC of CFS ensemble mean forecasts (a),(b) SST and (c),(d) precipitation at 0-month lead for the spring and winter seasons. (middle) HSS (%) for CFS forecasts of (e),(f) SST and (g),(h) precipitation at 0-month lead for the spring and winter seasons. (right) As in the middle panels, but for RPSS (%) for (i),(j) SST and (k),(l) precipitation. In (a)–(d) the contours denote statistically significant (95%) correlations.

along the equatorial Pacific is supported by the present analysis. Based on the lagged association between TIO and tropical Pacific SST anomalies, past seasonal prediction studies have used statistical methods to predict TIO SST anomalies (e.g., Mason et al. 1999). However, recent studies also suggest that these ENSO-induced regional SST anomalies may possibly alter the strength of the circulation and rainfall anomalies elsewhere (Annamalai et al. 2005b, 2007, 2010). The ability of CFS to represent the coupled processes in the TIO, particularly over SWIO during ENSO years, deserves further attention.

The predictive skill of regional precipitation, however, is usually lower compared to SST (Tables 2, 3)

and circulation (Kumar and Hoerling 1998) because of the “noisy,” small-scale character, and complex physics of precipitation. Even averaged over a season, substantial irregularities in the spatial pattern are likely, particularly over the tropics where convective rainfall is most common (Gong et al. 2003). Even so, observational and modeling studies suggest that the large-scale circulation pattern responsible for the precipitation anomaly may be predictable several months in advance, particularly during ENSO events. An examination of the spatial pattern of DJF SST and rainfall anomalies during all El Niño events indicates that CFS is capable of forecasting the “details,” in particular the observed negative



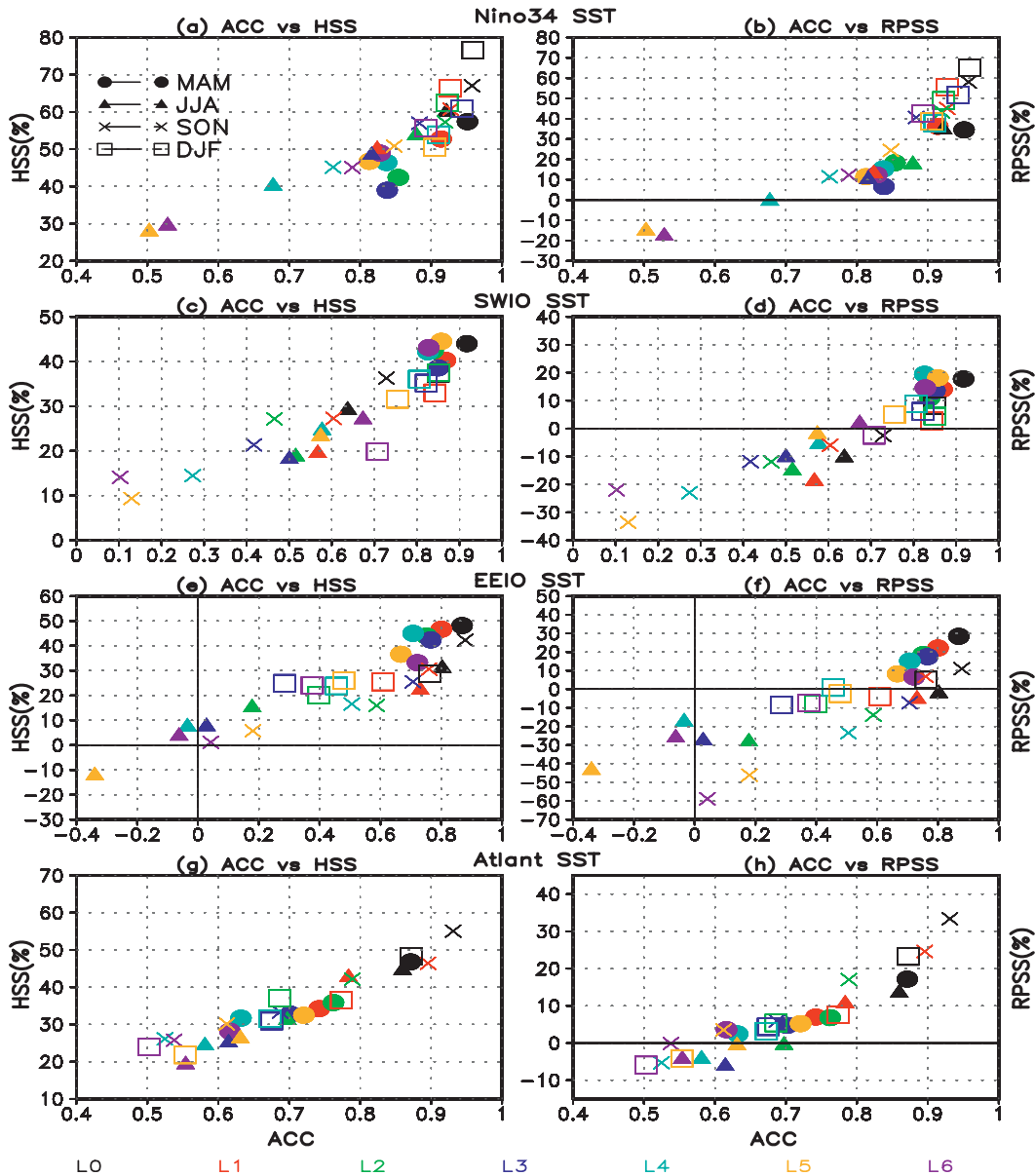


FIG. 14. Scatter diagram between (left) ACC and HSS and (right) ACC and RPSS for four standard seasons derived from CFS forecasts at 0–6-month leads: (a),(b) for Niño-3.4 SST, (c),(d) SWIO SST, (e),(f) EEIO SST indices, and (g),(h) Atlantic SST indices.

rainfall anomalies over all three USAPI regions during 1982/93 and 1997/87, as well above normal rainfall over Hawaii during the 1990–91 and 2004–05 events (figure not shown).

To date, the operational seasonal forecasting of precipitation over the USAPI stations relies on an empirical method in which precipitation measured at individual stations itself is treated as a predictor (He and Barnston 1996). The results of He and Barnston (1996) based on the period 1955–94 suggest that at 1-month lead, ACCs for predicting winter rainfall anomalies are  $\sim 0.4$ ,  $0.6$ ,

and  $0.4$  over the South Pacific, western Pacific, and Hawaiian regions, respectively (their Fig. 4). The dynamical forecast system based on CFS, on the other hand, demonstrates much higher skill at longer lead times over the USAPI (Table 3) when area-averaged fields are examined. Dynamical models represent the major components of the climate system (ocean, land, and atmosphere) and can incorporate linear and non-linear interaction processes among the components, and are expected to provide better seasonal forecasts than statistical models. A word of caution is that output from



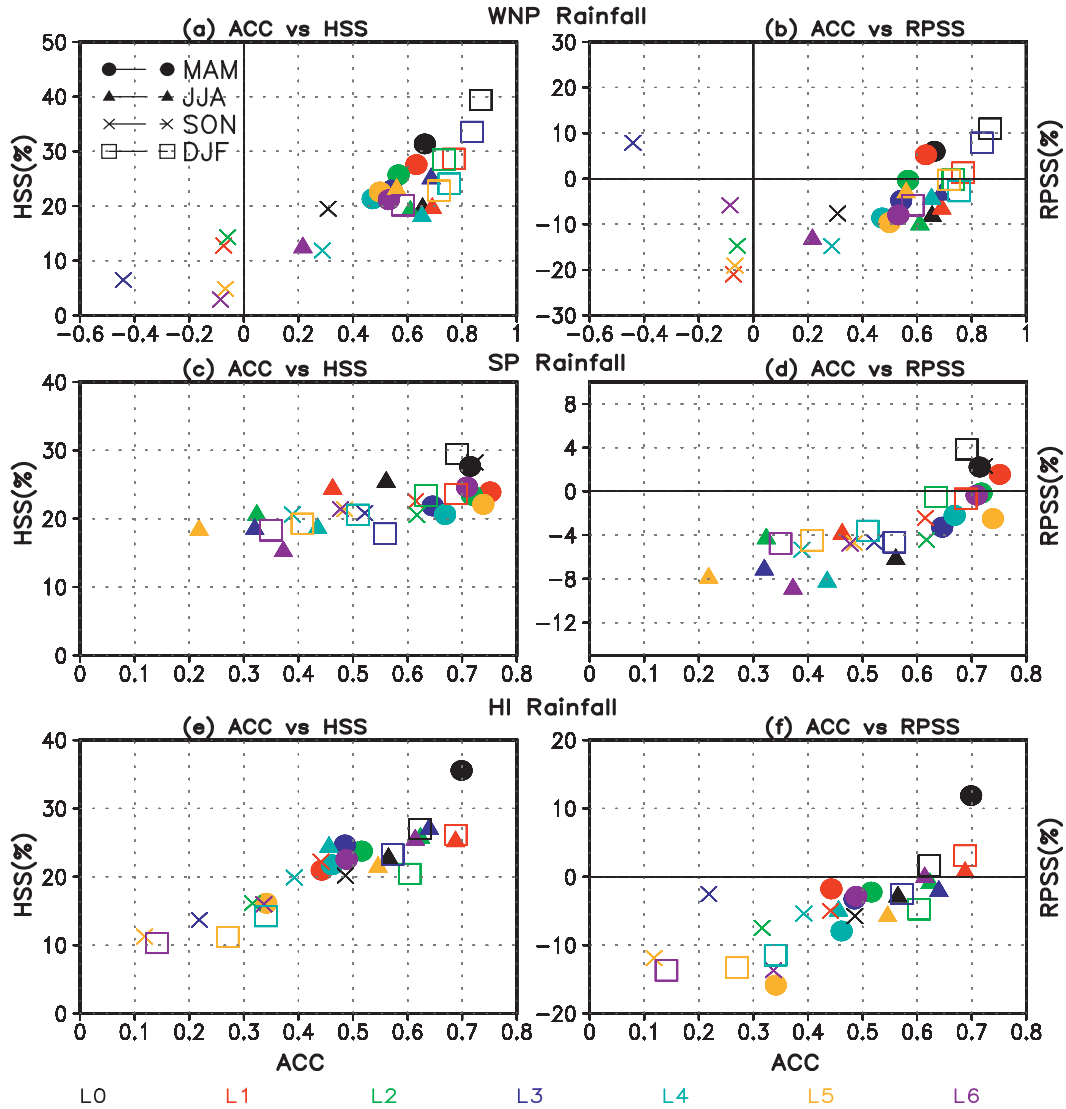


FIG. 15. As in Fig. 14, but for regional precipitation indices over (a),(b) the western North Pacific; (c),(d) the South Pacific; and (e),(f) HI.

CFS represents averages over a relatively coarse grid, and therefore statistics of precipitation in regions of steep orography can differ substantially from that of station data. Nevertheless, owing to the success of CFS in forecasting the timing and amplitude of ENSO-related SST and precipitation anomalies along the equatorial Pacific (Figs. 2, 7), and the associated teleconnection over the TIO (Figs. 7, 8), we speculate that CFS has useful skill in forecasting regional rainfall anomalies over the USAPI. However, identifying the individual physical processes responsible is beyond the scope of the present study. Lyon and Mason (2009) noted that the correct prediction of winter rainfall anomalies during 1998 over southern Africa by some coupled models is probably not for the correct reasons. Our future study

will examine the reasons for CFS performance over the USAPI.

### 7. Summary

In this study, the ability of CFS to forecast seasonal variations in SST and rainfall over the tropics is examined, first from the historical hindcasts for the period 1981–2005, and then for the real-time forecasts during 2006–09. A multitude of skill assessments, both deterministic and probabilistic, are employed in the analysis. This comprehensive analysis provides a useful guide to determining the skill and the associated errors of dynamical seasonal predictions of regional precipitation over the tropics, including over the USAPI. Probabilistic

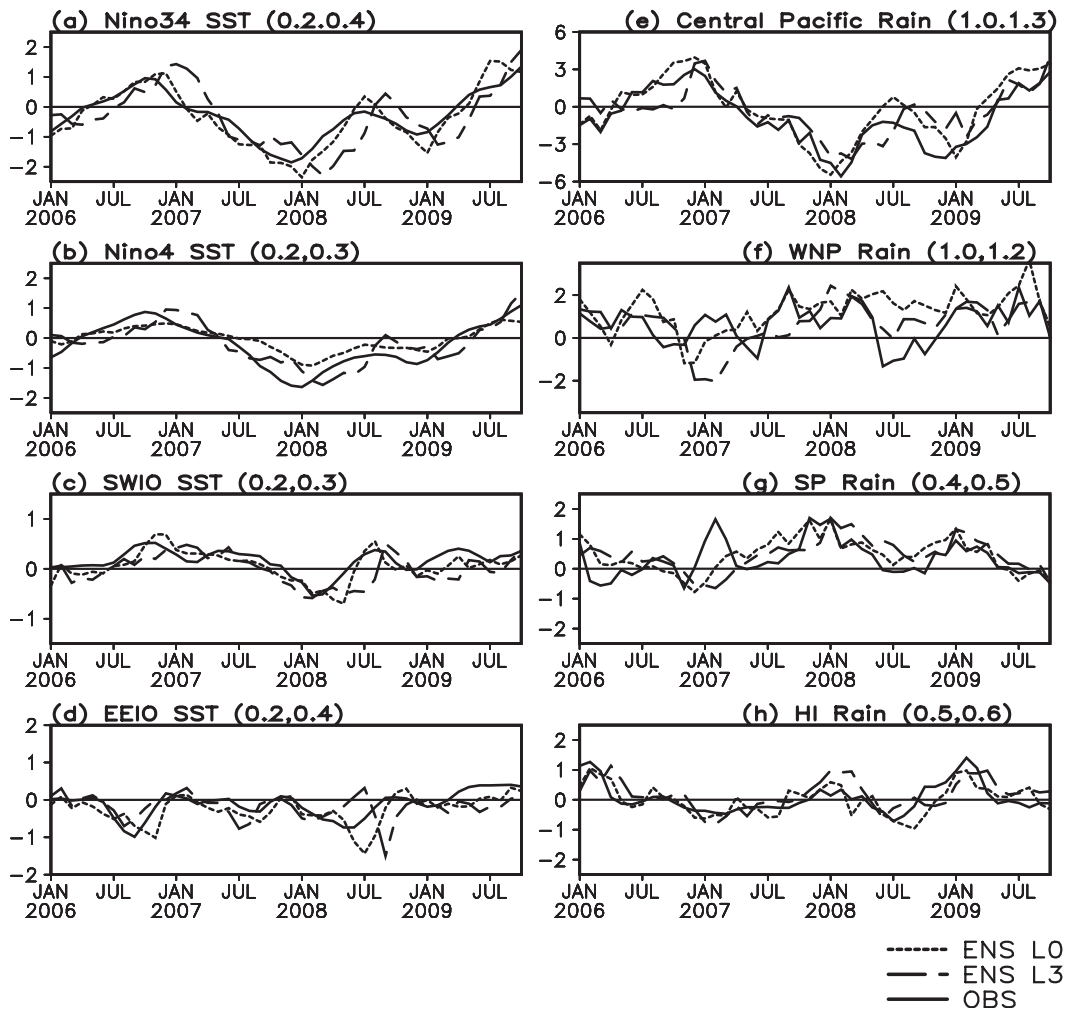


FIG. 16. (left) The 3-month average CFS ensemble mean real-time prediction of SST ( $^{\circ}\text{C}$ ) forecast at 0- (dotted) and 3- (dashed) month leads over the (a) Niño-3.4, (b) Niño-4, (c) SWIO, and (d) EEIO regions. The starting period is JFM of 2006, the next period is FMA of 2006, and so on. The corresponding observed SST is also shown (solid line). (right) As in the left panels, but for the precipitation ( $\text{mm day}^{-1}$ ) over (e) the central Pacific ( $5^{\circ}\text{S}$ – $5^{\circ}\text{N}$ ,  $150^{\circ}$ – $190^{\circ}\text{E}$ ), (f) the western North Pacific, (g) the South Pacific, and (h) Hawaii. The standard deviation and spread for the real-time prediction system are given in parentheses.

forecasts provide the means for predicting climate-related risk, and single deterministic forecasts, by contrast, are incapable of this (Palmer et al. 2004).

The model demonstrates high skill in forecasting the ENSO-related SST anomalies during the developing and mature phases, including that of different types of El Niño, even at 5–6-month lead (Figs. 2, 3, 13, 14a; Table 1a). It is sufficient to mention that CFS is capable of providing the necessary conditions for a successful prediction of seasonal climate anomalies. At 0–6-month lead, CFS captures the space–time evolution in SST, 850-hPa wind, and rainfall anomalies along the equatorial Pacific. Remarkably, the mechanisms involved in the teleconnection from the tropical Pacific to the tropical

Indian Ocean are well represented. Subsequently, CFS skill in predicting SWIO SST anomalies at longer leads is possible. The successful predictions of ENSO-related precipitation anomalies along the equatorial Pacific, and over the TIO, mean that the circulation and regional rainfall anomalies over the USAPI are better predicted.

A detailed examination of CFS ability in forecasting the regional rainfall anomalies over the USAPI indicates that the persistence dryness from El Niño winter into the following spring/summer is skillful and useful too. Quite remarkable is that the dryness can be predicted at leads longer than 3 months, and the fact that both deterministic and probabilistic skill scores converge

means that the forecast is useful (Table 3; Figs. 10–12, 15). Over the USAPI, the drought-like conditions during the strong El Niño winters of 1982/83 and 1997/98 were predicted by all of the ensemble members at 6-month lead itself (Figs. 10–12). Forecasting summer SST and precipitation anomalies along the equator is least skillful, as indicated by the higher spread among the ensemble members (low S/N) or negative RPSS values. Diagnostics of the real-time forecast for the period 2006–09 are generally in agreement with the hindcasts.

The results presented here suggest the feasibility that a dynamical system based seasonal prediction of precipitation over the USAPI can be considered. It is necessary to continually assess the sources and the level of prediction skill, as newer sets of hindcasts based on improved models and initial conditions obtained from more advanced data assimilation systems become available. For instance, one clear limitation in the hindcasts analyzed here is that for short-lead forecasts the initial conditions are from the old reanalysis system, a situation that would be rectified with the new CFS forecast model. In addition, in the updated CFS version the atmospheric model has a higher horizontal resolution (T126 compared to T62 in the current version), and may provide the better resolution necessary for precipitation prediction. In a future study, the physical processes that may be responsible for the performance of the model in predicting regional rainfall anomalies will be examined. To attain station-level predictions of rainfall anomalies over the USAPI, a downscaling system needs to be constructed.

*Acknowledgments.* The first author expresses his sincere gratitude to Jan Hafner, V. Prasanna, P. Pillai, J. Chowdary, H.J. Kim, and J.Y. Lee for various discussions during the course of this project. Comments from Drs. Chowdary and Pillai on the draft version of the manuscript are appreciated. Comments and critiques from the anonymous reviewers helped in improving the presentation of this manuscript. This study is supported by the NOAA Climate Test Bed (CTB) program and also partly funded by the institutional grants of the IPRC.

## APPENDIX

### HSS and RPSS Methods

#### a. HSS

For dichotomous forecasts, the HSS for time series of length  $n$  is defined as (Kumar 2009)

$$\text{HSS} = \frac{\left(F_c - \frac{N}{3}\right)}{\left(N - \frac{N}{3}\right)}, \quad (\text{A1})$$

where  $F_c$  is the correct number of forecasts (i.e., the number of cases when the observed category is also the forecast category) and  $N$  is the total number of instances the forecast was made. For the hindcasts analyzed here, we have 15 ensemble realizations. Using a counting procedure, we determine the number of ensemble realizations falling in each tercile category. The criteria for defining the tercile boundary is given by  $0.43 \times$  standard deviation of the variable. If  $n_1$  is the number of realizations for the forecasts to be in the below normal category, and  $n_2$  and  $n_3$  are numbers of realizations for the near-normal and above normal categories, respectively, then by definition,  $N = n_1 + n_2 + n_3 = 15$ , and the forecast category is the category for which  $N$  is the highest. We then compute HSS using Eq. (A1) based on the number of times the forecast category was correct.

#### b. RPSS

Rank probability skill (RPS) is computed as the sum of the squared differences between the cumulative distributions of the forecasts and observations. Similar to HSS, here too we obtained the number of ensemble realization ( $n_1$ ,  $n_2$ , and  $n_3$ ) for each tercile category, and the forecast probability for each category is defined as (i.e.,  $n_1/15$ ,  $n_2/15$ , and  $n_3/15$ ). RPSS basically measures the square error between the cumulative forecast probabilities for each category and the observed category relative to climatological forecast (Goddard et al. 2003 and references therein).

The RPS is defined as

$$\text{RPS} = \sum_{m=1}^{m=N} (f_m - o_m)^2, \quad (\text{A2})$$

where  $N = 3$  for tercile forecasts. Here,  $f_m$  represents the cumulative probabilities of the forecast up to category  $m$ , and  $o_m$  is the cumulative observed probability up to category  $m$ . The value of  $o_m$  is 100% for the observed category (e.g., normal) and zero for subsequent categories (above and below normal).

The RPSS (as mentioned above) measures the skill with respect to the climatology forecast (that assigns equal probabilities, 33.3% for each of the tercile categories) and is defined as

$$\text{RPSS} = 1 - \frac{\text{RPS}_{\text{fcst}}}{\text{RPS}_{\text{clim}}}, \quad (\text{A3})$$

where  $RPS_{\text{fcst}}$  is the RPS for the actual forecast and  $RPS_{\text{clim}}$  is the RPS of the climatological forecast.

## REFERENCES

- AchutaRao, K. M., and K. R. Sperber, 2006: ENSO simulation in coupled ocean–atmosphere models: Are the current models better? *Climate Dyn.*, **27**, 1–15, doi:10.1007/s00382-006-0119-7.
- Anderson, D. L. T., and J. P. McCreary, 1985: On the role of the Indian Ocean in a coupled ocean–atmosphere model of El Niño and the Southern Oscillation. *J. Atmos. Sci.*, **42**, 2439–2444.
- , and Coauthors, 2003: Comparison of the ECMWF seasonal forecast system 1 and 2, including relative performance for the 1997/8 El Niño. ECMWF Tech. Memo. 404, 93 pp.
- Annamalai, H., R. Murtugudde, J. Potemra, S. P. Xie, P. Liu, and B. Wang, 2003: Coupled dynamics in the Indian Ocean: Spring initiation of the zonal mode. *Deep-Sea Res. II*, **50**, 2305–2330.
- , P. Liu, and S. P. Xie, 2005a: Southwest Indian Ocean SST variability: Its local effect and remote influence on Asian monsoons. *J. Climate*, **18**, 4150–4167.
- , S. P. Xie, J. P. McCreary, and R. Murtugudde, 2005b: Impact of Indian Ocean sea surface temperature on developing El Niño. *J. Climate*, **18**, 302–319.
- , H. Okajima, and M. Watanabe, 2007: Possible impact of the Indian Ocean SST on the Northern Hemisphere circulation during El Niño. *J. Climate*, **20**, 3164–3189.
- , S. Kida, and J. Hafner, 2010: Potential impact of the tropical Indian Ocean–Indonesian seas on El Niño characteristics. *J. Climate*, **23**, 3933–3952.
- Barnston, A. G., M. H. Glantz, and Y. He, 1999: Predictive skill of statistical and dynamical climate models in SST forecasts during the 1997–98 El Niño episode and the 1998 La Niña onset. *Bull. Amer. Meteor. Soc.*, **80**, 217–244.
- , A. Kumar, L. Goddard, and M. P. Hoerling, 2005: Improving seasonal prediction practices through attribution of climate variability. *Bull. Amer. Meteor. Soc.*, **86**, 59–72.
- Battisti, D. S., 1988: Dynamics and thermodynamics of a warming event in a coupled tropical atmosphere–ocean model. *J. Atmos. Sci.*, **45**, 2889–2919.
- Charney, J. G., and J. Shukla, 1981: Predictability of monsoons. *Monsoon Dynamics*, J. Lighthill and R. P. Pearce, Eds., Cambridge University Press, 99–109.
- Clarke, A. J., and S. Van Gorder, 1999: The connection between the boreal spring Southern Oscillation persistence barrier and biennial variability. *J. Climate*, **12**, 610–620.
- , and —, 2003: Improving El Niño prediction using a space-time integration of Indo-Pacific winds and equatorial Pacific upper ocean heat content. *Geophys. Res. Lett.*, **30**, 1399, doi:10.1029/2002GL016673.
- Goddard, L., S. J. Mason, S. E. Zebiak, C. F. Ropelewski, R. Basher, and M. A. Cane, 2001: Current approaches to seasonal-to-interannual climate predictions. *Int. J. Climatol.*, **21**, 1111–1152.
- , A. G. Barnston, and S. J. Mason, 2003: Evaluation of the IRI’s “net assessment” seasonal climate forecasts 1997–2001. *Bull. Amer. Meteor. Soc.*, **84**, 1761–1781.
- Gong, X., A. G. Barnston, and M. N. Ward, 2003: The effect of spatial aggregation on the skill of seasonal precipitation forecasts. *J. Climate*, **16**, 3059–3071.
- Guilyardi, E., and Coauthors, 2004: Representing El Niño in coupled ocean–atmosphere GCMs: The dominant role of the atmospheric component. *J. Climate*, **17**, 4623–4629.
- He, Y., and A. G. Barnston, 1996: Long-lead forecasts of seasonal precipitation in the tropical Pacific islands using CCA. *J. Climate*, **9**, 2020–2035.
- Huang, B., and J. L. Kinter III, 2002: The interannual variability in the tropical Indian Ocean and its relations to El Niño–Southern Oscillation. *J. Geophys. Res.*, **107**, 3199, doi:10.1029/2001JC001278.
- Jin, E. K., and J. L. Kinter III, 2009: Characteristics of tropical Pacific SST predictability in coupled GCM forecasts using the NCEP CFS. *Climate Dyn.*, **32**, 675–691, doi:10.1007/s00382-008-0418-2.
- , and Coauthors, 2008: Current status of ENSO prediction skill in coupled ocean–atmosphere models. *Climate Dyn.*, **31**, 647–664.
- Kanamitsu, M., W. Ebisuzaki, J. Woollen, S.-K. Yang, J. J. Hnilo, M. Fiorino, and G. L. Potter, 2002: NCEP–DOE AMIP-II Reanalysis (R-2). *Bull. Amer. Meteor. Soc.*, **83**, 1631–1643.
- Kang, I.-S., and J. Shukla, 2006: Dynamical seasonal prediction and predictability of the monsoon. *The Asian Monsoon*, B. Wang, Ed., Springer, 586–612.
- Kao, H.-Y., and J.-Y. Yu, 2009: Contrasting eastern Pacific and central Pacific types of ENSO. *J. Climate*, **22**, 615–632.
- Kessler, W. S., M. J. McPhaden, and K. Weickmann, 1995: Forcing of intraseasonal Kelvin waves in the equatorial Pacific. *J. Geophys. Res.*, **100** (C6), 10 613–10 631.
- Kirtman, B., and A. Pirani, 2009: The state of the art of seasonal prediction: Outcomes and recommendations from the First World Climate Research Program Workshop on Seasonal Prediction. *Bull. Amer. Meteor. Soc.*, **90**, 455–458.
- Klein, S. A., B. J. Soden, and N. G. Lau, 1999: Remote sea surface temperature variation during ENSO: Evidence for a tropical atmosphere bridge. *J. Climate*, **12**, 917–932.
- Kug, J.-S., and I.-S. Kang, 2006: Interactive feedback between ENSO and the Indian Ocean. *J. Climate*, **19**, 1784–1801.
- , F. F. Jin, and S. I. An, 2009: Two types of El Niño events: Cold tongue El Niño and warm pool El Niño. *J. Climate*, **22**, 1499–1515.
- Kumar, A., 2009: Finite samples and uncertainty estimates for skill measures for seasonal prediction. *Mon. Wea. Rev.*, **137**, 2622–2631.
- , and M. P. Hoerling, 1995: Prospects and limitations of seasonal atmospheric GCM predictions. *Bull. Amer. Meteor. Soc.*, **76**, 335–345.
- , and —, 1998: Annual cycle of Pacific–North American predictability associated with different phases of ENSO. *J. Climate*, **11**, 3295–3308.
- Larkin, N. K., and D. E. Harrison, 2005a: Global seasonal temperature and precipitation anomalies during El Niño autumn and winter. *Geophys. Res. Lett.*, **32**, L16705, doi:10.1029/2005GL022860.
- , and —, 2005b: On the definition of El Niño and associated seasonal average U.S. weather anomalies. *Geophys. Res. Lett.*, **32**, L13705, doi:10.1029/2005GL022738.
- Latif, M., and Coauthors, 1994: A review of ENSO prediction studies. *Climate Dyn.*, **9**, 167–179.
- Livezey, R. E., M. Masutani, and M. Ji, 1996: SST-forced seasonal simulation and prediction skill for versions of the NCEP/MRF model. *Bull. Amer. Meteor. Soc.*, **77**, 507–517.
- Luo, J. J., S. Masson, S. K. Behera, and T. Yamagata, 2008: Extended ENSO predictions using a fully coupled ocean–atmosphere model. *J. Climate*, **21**, 84–93.
- , R. Zhang, S. K. Behera, Y. Masumoto, F. F. Jin, R. Lukas, and T. Yamagata, 2010: Interaction between El Niño and extreme Indian Ocean dipole. *J. Climate*, **23**, 726–742.



- Lyon, B., and S. Mason, 2009: The 1997/98 summer rainfall season in southern Africa. Part II: Model simulations and coupled model forecasts. *J. Climate*, **22**, 3802–3818.
- Mason, S. J., L. Goddard, N. E. Graham, E. Yulaeva, L. Sun, and P. A. Arkin, 1999: The IRI seasonal climate prediction system and the 1997/98 El Niño event. *Bull. Amer. Meteor. Soc.*, **80**, 1853–1873.
- Murtugudde, R., and A. Busalacchi, 1999: Interannual variability of the dynamics and thermodynamics of the tropical Indian Ocean. *J. Climate*, **12**, 2300–2326.
- Neelin, D. J., D. S. Battisti, A. C. Hirst, F. F. Jin, Y. Wakata, T. Yamagata, and S. E. Zebiak, 1998: ENSO theory. *J. Geophys. Res.*, **103** (C7), 14 261–14 290.
- Palmer, T. N., and Coauthors, 2004: Development of a European Multi-Model Ensemble System for Seasonal to Interannual Prediction (DEMETER). *Bull. Amer. Meteor. Soc.*, **85**, 853–872.
- Rao, S. A., S. K. Behera, Y. Masumoto, and T. Yamagata, 2002: Interannual subsurface variability in the tropical Indian Ocean with a special emphasis on the Indian Ocean dipole. *Deep-Sea Res. II*, **49**, 1549–1572.
- Reynolds, R. W., N. A. Rayner, T. M. Smith, D. C. Stokes, and W. Wang, 2002: An improved in situ and satellite SST analysis for climate. *J. Climate*, **15**, 1609–1625.
- Ropelewski, C. F., and M. S. Halpert, 1987: Global and regional scale precipitation associated with El Niño/Southern Oscillation. *Mon. Wea. Rev.*, **115**, 1606–1626.
- , and —, 1989: Precipitation pattern associated with the high index phase of the Southern Oscillation. *J. Climate*, **2**, 268–284.
- Saha, S., and Coauthors, 2006: The NCEP Climate Forecast System. *J. Climate*, **19**, 3483–3517.
- Shinoda, T., M. A. Alexander, and H. H. Hendon, 2004: Remote response of the Indian Ocean to interannual SST variations in the tropical Pacific. *J. Climate*, **17**, 362–372.
- Shukla, J., 1998: Predictability in the midst of chaos: A scientific basis for climate forecasting. *Science*, **282**, 728–731.
- , and M. Wallace, 1983: Numerical simulation of the atmospheric response to equatorial Pacific sea surface temperature anomalies. *J. Atmos. Sci.*, **40**, 1613–1630.
- Soman, M. K., and J. M. Slingo, 1997: Sensitivity of the Asian summer monsoon to aspects of sea surface temperature anomalies in the tropical Pacific Ocean. *Quart. J. Roy. Meteor. Soc.*, **123**, 309–336.
- Stockdale, T. N., and Coauthors, 2011: ECMWF seasonal forecast system 3 and its prediction of sea surface temperature. *Climate Dyn.*, **37**, 455–471, doi:10.1007/s00382-010-0947-3.
- Su, H., and J. D. Neelin, 2002: Teleconnection mechanism for tropical Pacific descent anomalies during El Niño. *J. Atmos. Sci.*, **59**, 3767–3781.
- Van Oldenborgh, G. J., M. A. Balmaseda, L. Ferranti, T. N. Stockdale, and D. L. T. Anderson, 2005a: Did the ECMWF seasonal forecast model outperform statistical ENSO forecast models over the last 15 years? *J. Climate*, **18**, 3240–3249.
- , —, —, —, and —, 2005b: Evaluation of atmospheric fields from ECMWF seasonal forecasts over a 15-year period. *J. Climate*, **18**, 3250–3269.
- Wajswowicz, R. C., 2005: Potential predictability of tropical Indian Ocean SST anomalies. *Geophys. Res. Lett.*, **32**, L24702, doi:10.1029/2005GL024169.
- Wang, B., and Coauthors, 2009: Advance and prospectus of seasonal prediction: Assessment of the APCC/CliPAS 14-model ensemble retrospective seasonal prediction (1980–2004). *Climate Dyn.*, **33**, 93–117, doi:10.1007/s00382-008-0460-0.
- Wang, G., and H. H. Hendon, 2007: Sensitivity of Australian rainfall to inter-El Niño variations. *J. Climate*, **20**, 4211–4226.
- Wang, W., M. Chen, and A. Kumar, 2010: An assessment of the CFS real-time seasonal forecasts. *Wea. Forecasting*, **25**, 950–969.
- Watanabe, M., and F. F. Jin, 2003: A moist linear baroclinic model: Coupled dynamical-convective response to El Niño. *J. Climate*, **16**, 1121–1139.
- Wilks, D. S., 1995: *Statistical Methods in the Atmospheric Sciences*. Academic Press, 467 pp.
- Wu, R., and B. P. Kirtman, 2004: Understanding the impacts of the Indian Ocean on ENSO variability in coupled GCM. *J. Climate*, **17**, 4019–4031.
- , —, and H. Van den Dool, 2008: An analysis of ENSO prediction skill in the CFS retrospective forecasts. COLA Tech. Rep. 264, 42 pp.
- Xie, P., and P. A. Arkin, 1996: Analysis of global monthly precipitation using gauge observations, satellite estimates, and numerical model predictions. *J. Climate*, **9**, 840–858.
- Xie, S.-P., H. Annamalai, F. Schott, and J. P. McCreary Jr., 2002: Structure and mechanisms of south Indian Ocean climate variability. *J. Climate*, **15**, 864–874.